HiLumi LHC

FP7 High Luminosity Large Hadron Collider Design Study

Deliverable Report

Compact Crab Cavity Cryomodule

Artoos, K (CERN) *et al*

13 October 2015

This work is part of HiLumi LHC Work Package **4: Crab cavities**.

Grant Agreement No: 284404

HILUMI LHC

FP7 High Luminosity Large Hadron Collider Design Study

Seventh Framework Programme, Capacities Specific Programme, Research Infrastructures, Collaborative Project, Design Study

DELIVERABLE REPORT

COMPACT CAVITY CRYOMODULE
DELIVERABLE: D4.4

Document identifier:	HILUMILHC-Del-D4-4-v2.0
Due date of deliverable:	End of July 2015
Report release date:	06/11/2015
Work package:	WP4: Crab Cavities & RF
Lead beneficiary:	CERN
Document status:	Final

Abstract:

The use of transverse deflecting cavities, known as crab cavities, was proposed in the LHC to correct the geometric effects of the large crossing angles as a consequence of the reduced beam sizes with the HL-LHC upgrade. This document details the functional requirements, RF and mechanical design of compact cavity cryomodule and the relevant RF services. Mechanical, thermal and operational aspects where relevant are described.

The information herein only reflects the views of its authors and not those of the European Commission and no warranty expressed or implied is made with regard to such information or its use.

Delivery Slip

	Name	Partner	Date
Authored by	K. Artoos[1], S. Atieh[1], K. Brodzinski[1], R. Calaga[1], O. Capatina[1], T. Capelli[1], F. Carra[1], L. Dassa[1], P. Freijedo Menendez[1], M. Garlasché[1], T. Jones[2], N. Kuder[1], S. Langeslag[1], R. Leuxe[1], A. Macpherson[1], E. Montesinos[1], M. Sosin[1], N. Templeton[2], G. Vandoni[1], G. Villiger[1], C. Zanoni[1]	CERN[1], STFC[2]	23/09/2015
Edited by	R. Calaga, C. Zanoni	CERN	23/09/2015
Reviewed by	L. Rossi, Project Coordinator E. Jensen, RF Group Leader G. Burt, WP4 co-coordinator	CERN STFC	28/09/2015
Approved by	Steering Committee		08/10/2015
Revised by	C. Zanoni	CERN	04/11/2015

TABLE OF CONTENTS

Executive summary

The use of transverse deflecting cavities, known as crab cavities, were proposed in the LHC to correct the geometric effects of the large crossing angles as a consequence of the reduced beam sizes with the HL-LHC upgrade. This document details the functional requirements, RF and mechanical design of compact cavity cryomodule and the relevant RF services. Mechanical, thermal and operational aspects where relevant are described.

1 INTRODUCTION

The LHC uses a 60 m common focusing channel on each side of the interaction region (IR) where the two counter-rotating beams have to be separated transversely to avoid parasitic collisions. The separation is accomplished by introducing a crossing angle at the interaction point (IP) which increases with the inverse proportionality of the transverse beam size at the collision point. The non-zero crossing angle implies an inefficient overlap of the colliding bunches. The luminosity reduction compared to that of a zero crossing angle, assuming a Gaussian distribution, can be conveniently expressed by a reduction factor,

$$R_\Phi = \frac{1}{\sqrt{1 + \Phi^2}},$$

where $\Phi = \sigma_z \phi / \sigma_x$ is the aspect ratio of the longitudinal (σ_z) to the transverse (σ_x) beam sizes multiplied by the half crossing angle ϕ or is also known as the Piwinski angle [1]. The reduction can be alternatively viewed as an increase in the transverse beam size at the collision point to effective beam size given by $\sigma_{eff} = \sqrt{\sigma_x^2 + \sigma_z^2 \phi^2}$. For HL-LHC beam parameters, the reduction compared to the case of a head-on collision can be 70% or larger. Therefore, the effective gain in luminosity by simply reducing the beam size at the collision point diminishes rapidly.

Figure 1: Bunches colliding with a crossing angle without (left) and with (right) the crab crossing.

To recover the loss, an elegant scheme using RF deflectors (also known as crab cavities) on either side of the collision point was first proposed and used for electrons [2, 3]. The time dependent transverse kick from an RF deflecting cavity is used to perform a bunch rotation in the $x - z$ plane about the barycentre of the bunch (see Figure **1**). The kick is transformed to a relative displacement of the head and the tail of the bunch at the IP to impose a head-on collision while maintaining the required beam separation to minimize parasitic collisions. The downstream RF deflector is used to reverse the kick to confine the bunch rotation to within the IR. The crab crossing scheme in a global compensation using only a single cavity per beam was successfully implemented at the e⁺e⁻ collider at KEKB in Japan to achieve record luminosity performance [4]. The geometrical correction was immediately accomplished, but the expected luminosity gain was not fully realized [4].

Since, the luminosity gain is substantial, the crab crossing scheme is adopted as a baseline of the HL-LHC upgrade. A time dependent transverse kick amplitude can be easily used to regulate the crossing angle. Therefore CC turns out to be a natural knob to control the total

number of events per crossing (luminosity levelling), a feature highly desired by the experiments. More sophisticated means of levelling to control the density of the events along the luminous region by means of crab cavities is under investigation [5].

1.1 BEAM AND RF PARAMETERS

The HL-LHC upgrade lattice requires crab cavities to provide a total voltage of 12-13 MV per beam per side of each collision point at a frequency of 400.79 MHz. Since the crossing plane in the two experiments is different, a local crab cavity system is a pre-requisite. A global scheme, even with a same crossing plane in the two experiments implies additional head-to-tail closed orbit oscillations propagating around the ring with potentially having a negative impact for aperture and machine protection. The nominal configuration will use a two-cavity cryomodule as a basic unit. Four such modules per IP side at P1 and P5 are required to perform the bunch rotation resulting in 16 modules (total 32 cavities). Four spare modules (8 cavities) are required, too. In IP1 the 4×2 modules are designed for vertical crossing, while in IP5 they are designed for horizontal crossing. A hybrid scheme with 2-horizontal and 2-vertical modules at each IP with increase kick strength is also considered as an alternate option for linear pile up density as mentioned above. The low frequency is required to minimize the RF curvature for the long LHC bunches angle (See Table 1). The machine constraints near the interaction region require cavities with a transverse dimension compatible with the location of the adjacent beam pipe. The RF and machine parameters directly relevant to the crab cavities are shown in Table 1.

Table 1: Relevant RF parameters for HL-LHC crab cavities

Characteristics	Units	Value
Resonance frequency	MHz	400.79
Bunch Length	ns	1.0 (4σ)
Maximum cavity radius	mm	≤ 145
Nominal kick voltage	MV	3.4
R/Q (assumed, linac convention)	Ω	400
Q_0		$\geq 1 \cdot 10^{10}$
Q_{ext} (Fixed coupling range)		$3 \cdot 10^5 \cdots 5 \cdot 10^5$
RF Power	kW	80
Power coupler OD (50Ω)	mm	62
LLRF Loop Delay	μs	≈ 1
Cavity detuning	kHz	≈ 1.0

The operating temperature of 2 K is chosen as a baseline. A pressure stability of on the cavity surface should be minimized to less than 1 mbar. The static and dynamic heat load is expected to be approximately 30 W to the 2 K bath for a two-cavity module. A cavity vacuum level to better than 10^{-10} mbar is required to assure stable performance.

The input RF power of 80 kW is available to power each of the 8 cavities to their nominal voltage with sufficient margin to cope with beam loading caused by beam offset. The Low Level RF (LLRF) will include a regulation loop around the tetrode (to reduce the RF amplitude and phase noise in a band extending to few tens of kHz), plus an RF feedback to control the vector sum precisely on the two sides of the interaction region. Longitudinal PUs located close to the crab cavities (one per IP-side per beam) are used to regulate the slow drifts of the

deflecting voltage with respect to the average bunch centre. To stay within the specified RF power limits, an orbit stability including mechanical tolerances must not exceed 1 mm with stable beams at flattop. The cavity is kept on tune at all times. The resonant frequency should be precisely controlled by a tuning system to a level well below 0.5 kHz to be compatible with the RF power limits.

2 RF CAVITY DESIGN

In order to sustain the surface fields at the required kick gradient of 3.4 MV/cavity for LHC crab crossing superconducting technology is essential; space restrictions, voltage requirements and impedance considerations strongly rule out a normal-conducting option. "Conventional" superconducting elliptical cavities, similar to the ones already used at KEK, pose very significant integration problems at the operating frequency of 400 MHz in the LHC due to their transverse size.

2.1 GEOMETRICAL CONSTRAINTS

Measuring from the electric centre line of the cavity (where the integral $\int_{-\infty}^{\infty} E_z e^{j\frac{\omega}{c}z} dz$ of the operating mode vanishes), the beam pipe at both ends of the cavity must leave a disk of radius 42 mm clear. This will allow the transverse alignment of the cavity without reducing the aperture for the beam. To allow passage of the 2nd beam it is required that the transverse space a distance of >145 mm from the electric centre line is kept clear for the passage of the 2nd beam pipe.
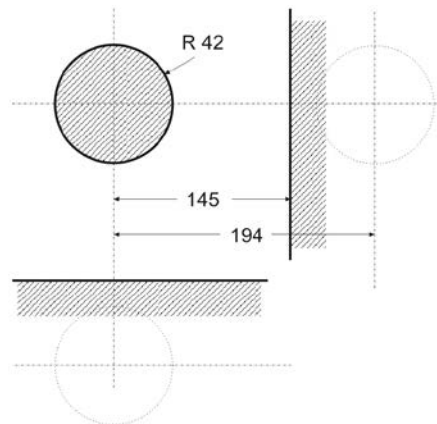
Figure 1 Schematic of the beam pipe separation and the maximum allowed cavity envelope in the LHC.

Since the 2nd beam pipe is at a distance of 194 mm horizontally for both cases, horizontal and vertical dipole kick, the cavity has to be designed that the passage for the 2nd beam pipe is assured for either direction of the dipole kick.

2.2 FREQUENCY & KICK VOLTAGE

At the LHC, the nominal cavity operating frequency is 400.790 MHz. For the SPS tests, the resonance frequency of the cold (2 K) cavity, fully equipped with couplers, probes and HOM dampers, must be tuneable with the tuner (described below) at least from 400.730 MHz to 400.850 MHz, i.e. to the nominal operating frequency ±60 kHz. Note that as testing of bare cavities in a vertical test setup at low power (SM18) may not have the full set of couplers

implemented, prototype cavities are to be tuned to this nominal LHC operating frequency. This should take into account the frequency changes from material removal during surface treatment, volume contraction during cool-down and other cavity manipulations.

The nominal cavity gradient per cavity is 3.4 MV of integrated kick resulting in a total of 12-13 MV in the LHC, with 4 cavities per beam per IP side [3]. Assuming a geometry factor of $G = 100\ \Omega$ and a cavity quality factor $Q_0 = 10^{10}$ the surface resistance $R_s = 10\ n\Omega$. The unloaded quality factor Q_0 for the cavities should aim at reaching a total surface resistance of $\leq 10\ n\Omega$ for their respective geometry factors. Nominal operation with the beam on axis of the deflecting cavity should lead to minimal or zero beam loading. Therefore, only a small amount of RF power is required to sustain the field in the cavity.. However, to accommodate non-zero beam loading from orbit error and frequency changes from external forces, the Q_L is significantly lower. Assuming $Q_L \approx Q_{ext,}$ the Q_{ext} will be adjusted so that $(R/Q) \cdot Q_{ext}$ is constant for all three candidates, and is defined by the available RF power and beam loading tolerances.

2.3   COMPACT CAVITY DESIGNS

This led to the concept of "compact" cavities. These cavities have unconventional geometries not widely used in superconducting technology. A few concepts with complex shapes exist primarily in the field of heavy ion acceleration. Such structures fit within the LHC constraints in the existing tunnel and reveal significantly better surface field characteristics than the conventional cavities for beam deflection. As a result of an intense R&D program within the EuCARD and LARP programs and with other external collaborators during the past 4 years, three compact designs at 400 MHz have emerged as potential candidates. Their topologies are shown in Figure **2**. The three proposed designs are at least 4 times smaller in the plane of crossing compared to an elliptical cavity with a ratio of the kick gradient to the peak surface fields lower by a factor of 2.
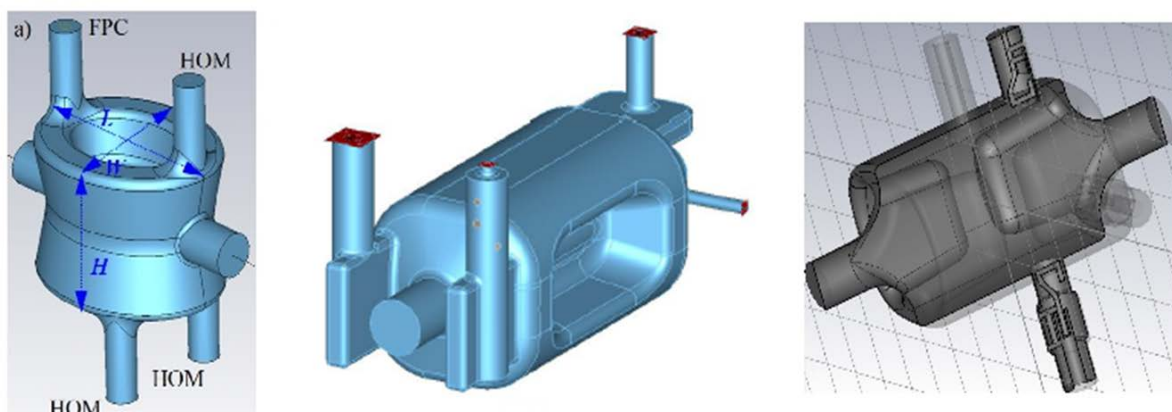
Figure 2: Compact cavities: a): Double quarter wave cavity (DQW) b): RF dipole cavity (RFD) c): 4-Rod Cavity (Courtesy Brookhaven National Lab, Old Dominion University and Lancaster University).

As a part of the R&D phase, it was determined to prototype the three full-scale designs for a field validation at the nominal kick voltage. Following the recommendation by the Crab Cavity Advisory Panel a prototype module in a two-cavity configuration will be tested with beam in the SPS machine with LHC type beams [6]. These tests will help validate the cavity performance and operation with beam and understand the effects on protons as well as relevant

machine protection aspects. The three cavities were fabricated in 2012-13 and their performance validated at or beyond the nominal kick voltage [7,8,9]. The cavity designs including the fundamental power coupler and higher order mode couplers have evolved significantly from the prototype to meet the impedance requirements of the LHC. Following the recommendation of the May 2014 technical review [Ref: 10], only two cavity designs are considered towards the SPS tests (DQW & RFD).

The development of a two-cavity cryomodule for the SPS tests in 2017 is at an advanced stage. An overview of the Crab Cavity Planning spanning approximately 10 years until the full installation in the LHC is shown in Table 2. A more detailed planning both the SPS and the LHC including the pre-series and series production can be found in [Ref: 11]

Table 2: Overview of Crab Cavity Planning from R&D to installation in the LHC.

2013-2014	2015-2017	2017-19	2019-2024	2024-25
Cavity Testing & Prototype Cryomodule	SPS Cryomodule Fabrication	SPS Tests & LHC Pre-Series Module	LHC Cryomodule Construction & Testing	LHC Installation

2.4 BEAM LOADING AND RF POWER

In deflecting cavities operated in the crabbing mode, the RF phase and the RF component of the beam current are in quadrature ($\phi_s = 0$, synchrotron convention). For a beam transversely centred, there is no beam loading: the RF generator does not pass power to the beam. With a superconducting cavity (negligible surface losses) the needed RF power to maintain the cavity voltage decreases monotonically with Q_L. Therefore, with a perfectly centred beam, the choice of Q_L only requires sufficient bandwidth for unavoidable frequency transients due to external perturbations (see section- frequency tuning).

The situation is different for a beam circulating at an offset Δx. The beam induced voltage due to an orbit offset is given by

$$\Delta V = I_B \cdot \frac{R_T}{Q_0} \cdot Q_L \cdot \Delta x$$

where, I_b is the average beam current, $\frac{R_T}{Q_0} \cdot Q_L$ is the transverse shunt impedance in Ω and the Δx is the offset. A sufficient bandwidth and the corresponding RF power are required to compensate for the unavoidable orbit offsets. Figure 3 shows the required forward power as a function of the Q_L for a beam that is centred (red) and off-centred by 1 mm (green) and 2 mm (blue). It is expected that the orbit will be kept within 0.5 mm for the entire energy cycle of the LHC; another 0.5 mm should be added for mechanical tolerances.
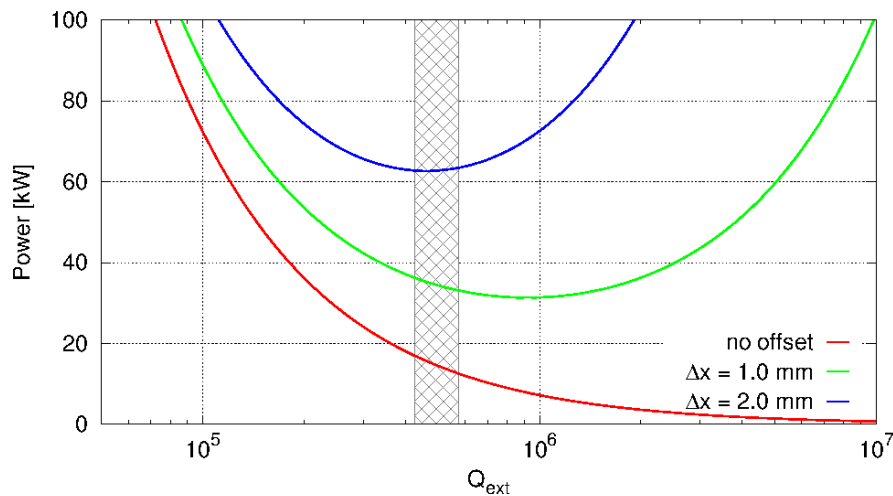
Figure 3: Forward power vs. cavity Q_L for centered (red) and $1\ mm$ offset (green) and $2\ mm$ offset (blue) beams. Assumed $R/Q = 400\ \Omega$, $3.4\ MV\,RF$, $1.1\ A\,DC$.

The required RF power has a broad minimum (≤ 40 kW) from a Q_L of about $3 \cdot 10^5$ to $1.5 \cdot 10^6$ for an offset specification of 1mm. Selection of an optimal Q_L value in the broad minimum is a compromise between the feasible tuning precision and the minimization of the field fluctuations from the amplifier electronic. For larger bandwidth (leading to more stability), lower Q_L values are favoured – the hashed area in Figure 3 was chosen a compromise. A lower Q_L is also favourable for the tuning system as it relaxes the precision needed by a mechanical system and the power needed to compensate for fast frequency changes.

2.5   RF POWER COUPLER

The RF power coupler was designed in view of the HL-LHC requirements; additional constraints (common platform) were introduced to limit the variances between the alternative designs in view of the SPS tests. The crab cavity power coupler will use a single coaxial disk window type to separate the cavity vacuum and the air side. The antenna shape is specific to each cavity as the coupling mechanisms to the different cavities are not identical. However, a common platform starting from the cavity flange followed by the ceramic and double wall tube is imposed. To respect the common platform, the inner antenna is dimensioned to 27 mm diameter with the outer coaxial line of 62 mm diameter for a maximum power capability of approximately 200 kW. The inner line is made of a copper tube and the outer line is Stainless Steel 316LN with inner surface coated with copper. The vacuum to air separation is achieved with a coaxial ceramic window (Al_2O_3) with the outer flange made of titanium. The rest of the items are built from massive OFE 3D forged copper blocks. The coupler body is made of a conical line to increase the near the ceramic region to limit arcing with the primary aim to enlarge the air side to the maximum while keeping the 62/27 mm dimensions for the input antenna in the vacuum side. A coaxial to waveguide transition is performed with a WR2300 half-height without a doorknob (see Figure 4).

The air side of the coupler will be air-cooled while the antenna itself will be water-cooled. The waveguide design includes the possibility of a DC polarisation in order to avoid multipacting effects. Each coupler is equipped with three ports for a vacuum gauge, electron monitoring and arc detection devices. The vacuum gauge, mandatory to protect the window during conditioning as well as in operation, will be oriented along the air line in order to minimize the cryomodule flange size. Special test boxes to condition the couplers are also designed (see Figure 4). The

Coupler ports are designed to come out on the top, perpendicular to the beam axis for ease of integration with the WR2300 waveguide transition. The cavity Helium vessel is designed to withstand the weight of the couplers and the waveguide (approx. 35 kg). The alternating crossing angle scheme will require that the orientation of a coupler assembly be robust for horizontal and vertical deflections.
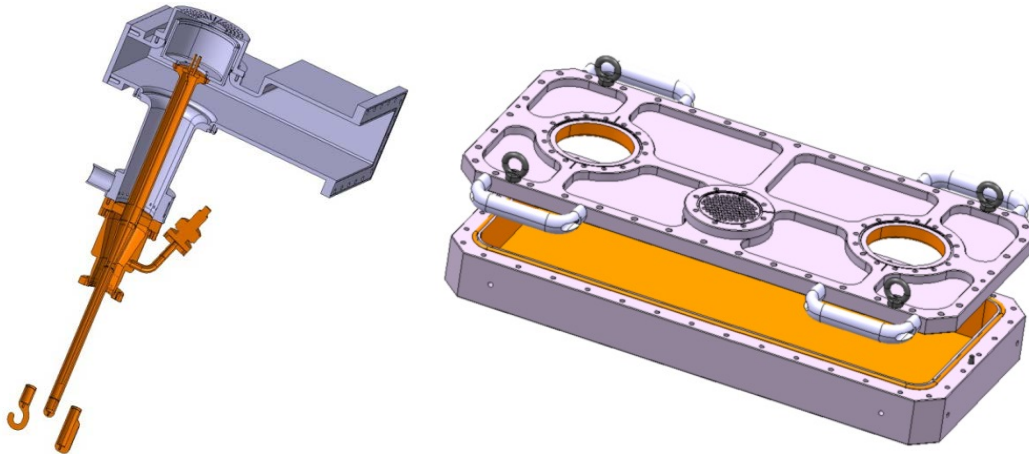

Figure 4: Input coupler assembly (left) and the test box for RF conditioning.

2.6   COUPLED BUNCH INSTABILITIES

The crab cavities must cope with the various modes of the collider cycle: filling, ramping and physics. During filling of the 2808 bunches into the LHC, ramping or operation without crab cavities (crabbing off), the cavity can be detuned, but a small field should be kept for the active tuning system. This is referred to as "parking". Parking the cavity half distance between two revolution frequency sidebands would be ideal for stability. Another possibility to operate with "crabbing off" is possible since more than one cavity is used, namely counter-phasing to make the effective kick voltage zero while always keeping accurate control of the cavity field. This counter-phasing ensures both zero effective voltage and beam stability on tune – in fact it is found that this is the preferred scenario [12].

If detuning is used with a positive non-integer tune ($Q_h = 64.3$), the cavity should be tuned above the RF frequency to make the mode $l = -64$ stabilizing (see Ref. [12]). Though RF feedback is not mandatory for stability with a detuned cavity, it is preferred for accurate knowledge and control of the cavity resonance frequency and field. Active feedback will also keep the beam induced voltage zero if the beam is off-centred. The additional RF power is used as a measurement of beam loading to guide the beam centring. The RF signal picked up through the HOM couplers, might also be used.

On the flattop detuning can be reduced (but keeping the total kick voltage at zero initially). The RF feedback keeps the cavity impedance small (beam stability) and compensates for the beam loading as the cavity moves to resonance. Once the cavity detuning is reduced to zero, we drive counter-phasing to zero and use the functions to synchronously change the voltage in all crab cavities as desired (crabbing on). In physics run, with the crabbing on, the active RF feedback will continue to provide precise control of the cavity field. The RF feedback reduces the peak cavity impedance and transforms the high Q resonator to an effective impedance that covers several revolution frequency lines. The actual cavity tune has no big importance for stability

anymore. The growth rates and damping rates are much reduced, and we have no more dominant mode as shown in Figure 5.
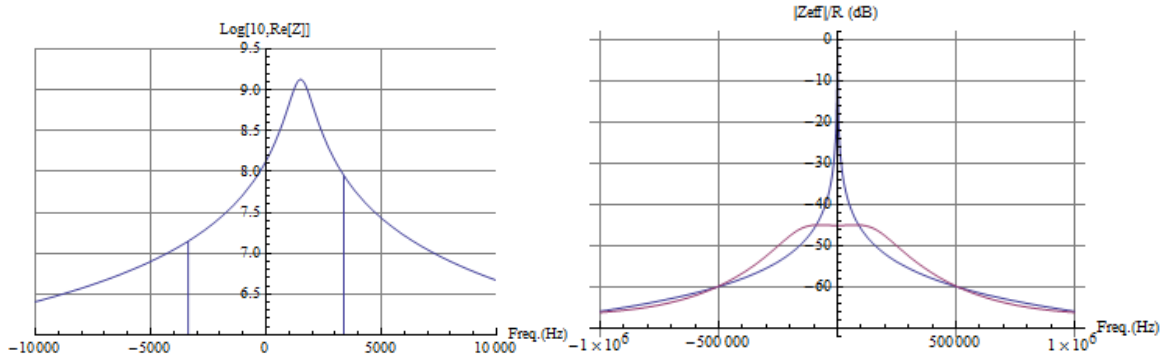

Figure 5: Left: Real part of the deflecting mode impedance with a detuning of 1.5 kHz from from 400 MHz. The vertical lines represent the difference in $\Re\{Z\}$ evaluated at $\pm 0.3\, f_{rev}$ for the computation of damping rate (mode l=-64). Right: Modulus of the cavity impedance seen by the beam with the RF feedback on (red) and off (blue) normalized to the cavity impedance at the fundamental mode.

2.7 IMPEDANCE BUDGET

On resonance, the large impedance of the fundamental deflecting (dipole) mode is cancelled between the positive and negative sideband frequencies, which are symmetric around ω_{RF}. The active feedback will reduce the growth rates by a large factor. For higher order modes (HOMs), both narrowband and broadband impedance should be minimized during the entire machine cycle as the LHC will accelerate and store beams of currents exceeding 1.1 A (DC). Tolerances are set from impedance thresholds estimated from Ref. [13].

The longitudinal impedance has approximately a quadratic behaviour vs. f in the region of interest with the minimum threshold value at 300–600 MHz The total maximum allowed impedance from each HOM, summing over all cavities in one beam, assuming that the HOM falls exactly on a beam harmonic, is set at <200 kΩ, so if all 16 cavities have identical HOM frequencies, the longitudinal impedance must not exceed 12.5 kΩ per cavity. For frequencies higher than 600 MHz, the threshold is higher ($\propto f^{5/3}$), but the same threshold was imposed. Modes with frequencies above 2 GHz are expected to be Landau-damped due to natural frequency spread and synchrotron oscillations.

In the transverse plane, the impedance threshold is set by the bunch-by-bunch feedback system with a damping time of $\tau_D = 5$ ms [13]. Eight effective cavities per beam per transverse plane (16 total per beam) are assumed due to the alternate crossing angles at the two experiments. The single bunch studies show that integrated R/Q over the frequency for all the HOMs per cavity should be suppressed to below 2 kΩ/m (without accounting for β-function) from stability considerations [**15**]. From multi-bunch considerations and assuming the pessimistic case that the HOM frequency coincides with the beam harmonic and identical HOM frequencies between the cavities, the maximum total impedance in each plane is set to be 160 kΩ/m [**15**]. Assuming well separated HOM spectrum and including β^*-leveling, the allowed impedance per cavity can be relaxed to 0.5 MΩ/m. Analogous to the longitudinal modes, frequencies above 2 GHz are expected to be Landau-damped due to natural frequency spread, chromaticity, and Landau octupoles.

Due to the very tight impedance thresholds, the distribution of HOM frequencies as mentioned above due to manufacturing errors can help relax the tolerances. The beam power deposited in the longitudinal HOMs can become significant when the frequencies coincide with bunch harmonics. The HOM couplers were dimensioned to accept a maximum of 1 kW to be able to cope with HL-LHC beams [31].

2.8   HOM COUPLERS

The first design goal of the HOM filter is to block the transmission of the main deflecting mode, while transmitting all remaining HOMs. Several HOM coupler designs were developed and optimized for different cavity geometries. Two high-pass filter designs, incorporating a notch filter at the fundamental frequency are shown in Figure 6 with both HOMs using hook-like antennas to couple to the HOMs.

Simulations show that the HOM coupler must have a superconductive surface due to the high fields of the fundamental mode. A second design constraint requires the HOM couplers to be able to efficiently remove the power in the HOMs (up to 1 kW) and the heat dissipated by the fundamental mode in the inner part of the HOM coupler from the cavity. High purity bulk niobium with sufficient cooling can ensure this. The required cooling may be possible via conduction, but the possibility to actively cool with superfluid liquid helium or immersion in a small LHe vessel is also under study.
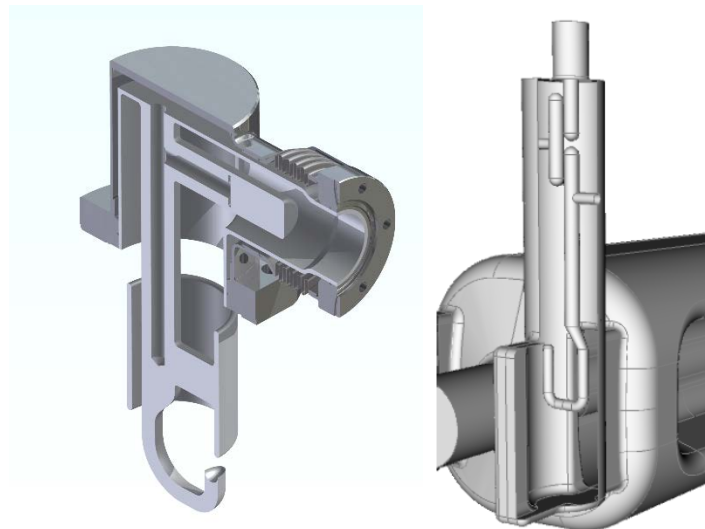
Figure 6: HOM filter for the DQW (left) and RFD (right).

2.9   RF MULTIPOLES

The crab cavity designs presently considered do not have axial symmetry. Therefore, they can potentially exhibit all higher order components of the main deflecting field. Due to the placement of the cavities at high beta-function locations, the higher order components of the main deflecting mode can affect long term particle stability. RF multipole components b_n of the RF deflecting field can be approximated and hence expressed in a similar fashion to

magnets[1] [32]. The quadrupolar component b_2 is zero in case of perfect symmetry; due to fabrication errors and ancillary components it is non-zero – it must be smaller than 10 units leading to a tune shift in the order of $\Delta Q \approx 10^{-4}$. The first systematic multipole is the sextupolar component, b_3. Long term simulations with the optical functions of the HL-LHC indicate that the b_3 component should be limited to approximately $1000 \pm 10\%$ units which results in an acceptable degradation of the dynamic aperture below 1σ for orbit offsets of 1.5 mm [12]. No specifications are provided for higher order terms yet, but it is expected that they be controlled to smaller values than the neighbouring D2 dipole magnet.

For $n \geq 4$, assuming a very approximate scaling of the additional kick from an orbit offset via b_n, the b_n must be kept $< \mathcal{O}(10^n)$. Better estimates are pending; results from long-term tracking are needed.

2.10 LORENTZ FORCE DETUNING & MULTIPACTING

When the cavity contains RF fields there is a Lorentz force on the cavity surface resulting from the high radiation pressure on the cavity walls. This results in a detuning of the cavity frequency. The Lorentz force detuning is kept small (≤ 0.6 kHz) at the nominal field.

Another common problem in complex RF structures is multipactor. This is a resonant electron phenomenon where an electron follows a regular trajectory in the RF fields where it strikes the surface with energy such that the number of secondary electrons produced is statistically likely to be greater than one. If these secondaries follow the same trajectory then the process will repeat causing an exponential growth in the number of secondaries. The electrons will absorb RF power limiting the field to a finite level and depositing additional heat load in the walls. Initially the cavity surface may have an oxidised layer which will increase the secondary electron yield (SEY). However multipactor also conditions the surface removing this layer. If the multipactor disappears after processing or if sufficient power is available to overcome the multipactor it is termed a "soft" barrier, otherwise it is termed a "hard" barrier.

Multipactor was modelled in all cavities and couplers using two codes using different methodologies to identify multipactor. CST Particle Studio uses particle tracking with accurate secondary emission models to simulate the growth in electrons with time, while Track3P tracks a single particle in the RF fields and looks for resonant trajectories.

In CST three SEY models were used to look at the effect of surface cleanliness. The models were for wet treated, baked and processed niobium surfaces. While multipactor in all cavities was found for the wet-treated and baked models, no multipacting trajectories were found for the processed surface, suggesting that any multipactor would be soft and easily processed through. Similarly Track3P found multipactor at low field. This is in good agreement with the results from the prototype tests, where multipactor was observed and could be processed away easily.

3 INTRODUCTION TO THE DRESSED CAVITIES

The sum of cavity with couplers and of the systems required around it in order to provide stiffness, cryogenic temperature, tuning and shielding from magnetic field is called dressed

---

[1] Definition of b_n: $b_n = \int_0^L \frac{1}{qc} F_\perp^n \, \mathrm{d}z$ in units of T m^{2-n}.

cavity. The temperature needed in the cavity is decided in function of the BCS resistance of Niobium. Such resistance at 4.5 K and 400 MHz is around 50 nΩ, which is more than 10 times larger than the value at 2 K. The complex shapes of the cavities may also be susceptible to microphonics caused by LHe boil-off, hence operation below the lambda point of He is preferred. For these reasons, operation at 2 K is baseline. This will require the provision of He II at 2 K to the crab cavity location in LHC. The heat load limits for LHC are not currently known, but is likely to be around 3 W of dynamic load per cavity at 2 K.

Following the recommendation of the May 2014 Crab Cavity International review [10], only two cavity designs are considered for the engineering development towards the SPS tests (DQW & RFD). The mechanical design of the cavities ensures their safe use under maximum loading condition during its entire life cycle. The cavity is dimensioned to cope with several mechanical constraints: ensure elastic deformation during maximum pressure as well as during all transport and handling conditions; maximise tuning range; minimise sensitivity to pressure fluctuation; avoid buckling due to external pressure; maximise the frequency of the first mechanical natural mode. The final mechanical design of the cavities including all external interfaces is shown in Figure 7. In summary, each cavity is equipped with: a helium tank, a tuning system, a fundamental RF power coupler, a field probe and two (RFD) or three (DQW) HOM couplers.
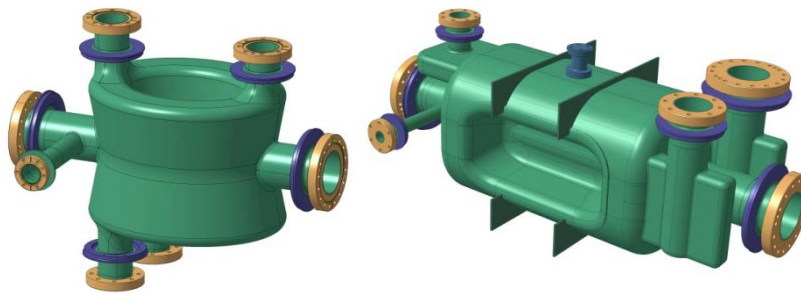

Figure 7: Schematic view of the cavity with interfaces (left: DQW & Right: RFD).

3.1   CAVITY MATERIAL & TREATMENT

The cavity fabrication is performed from bulk niobium sheets by electron-beam welding of deep-drawn parts. High purity bulk Niobium with a Residual Resistivity Ratio (RRR) >300 with the cavity surface fully annealed is recommended. Material should conform to R04220-Type 5 as per ASTM B393-09e1 with additional and overriding requirements as specified in this document. Chemical composition for main impurities should be limited to the amounts listed in Table 3.

Table 3: Impurities tolerance for cavity material.

Element	Max Content wt%
Ta	0.050
W	0.007
Ti	0.005
Mo	0.005
All other metallic impurities, each	0.003
H_2, N_2, O_2, C	0.001

A final thickness of 4 mm is calculated to be acceptable in order to cope with all the mechanical constraints as well as minimizing the cost of the cavity production. The cavities are cooled in a bath of saturated super-fluid helium at 2 K. The cavities undergo the standard chemical treatment of $150 - 200 \, \mu m$ of the cortical layer removal after the cavity fabrication. A rotational mechanism is preferred to ensure more uniform removal with the surface temperature controlled to $5 - 10^0 \, C$. Heat treatment for hydrogen degassing to avoid hydrogen disease should be followed after the bulk acid etching. It is typically performed at 600-650 °C for greater than 24 h, until equilibrium of the vacuum pressure is reached in the furnace. A Hydrogen concentration of 1 ppm at a pressure of less than 10^{-7} mbar is a reasonable target. After heat treatment, a light chemical etching to remove a thin layer of $10 - 15 \, \mu m$ should be performed to remove any impurities deposited on the surface. As a final step, the cavity undergoes a high pressure water rinse before the assembly of the cavity components in a clean room environment. All additional cavity parts undergo an ultra-sonic cleaning prior to the assembly.

3.2 PRESSURE VESSEL CODE

In the frame of SAPOCO 42 at CERN (defining the Organization's policy in terms of safety), the safety regulations on mechanical equipment (SR-M) [7] applies, supported by the general safety instructions for standard pressure equipment (GIS-M2) [8]. In particular, the European directive 97/23/EC [9] provides the health and safety requirements for pressure equipment. According to which specific requirements apply, the pressure equipment is classified into four categories (*I-IV*) to define the limits of applicability. In each design, the determination of the category has to be carried out to appropriately place the pressure equipment and conform to those requirements.
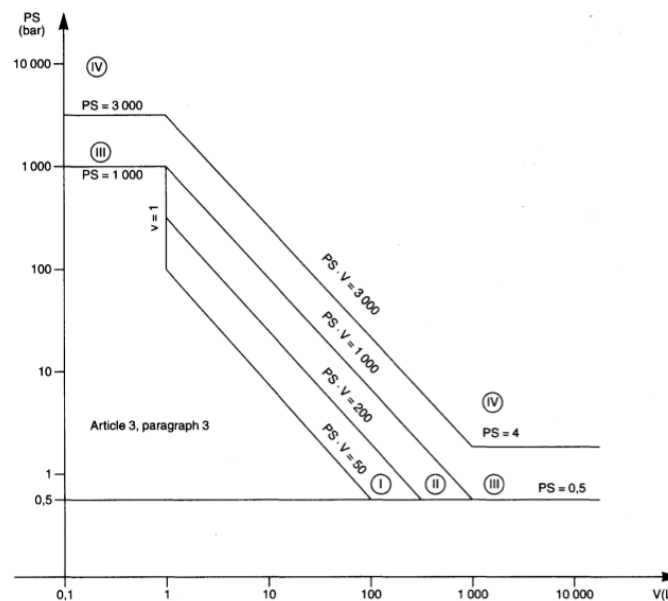

Figure 7: Assessment of risk category (European Directive 97/23/EC).

In a horizontal cryostat configuration, the pressure equipment will consist of several layers outside the cavity body. The first enclosing vessel is the Helium Tank maintained at 2 K. This vessel will be shielded with additional copper thermal shields at 80 K and any additional magnetic shields. The outer most steel shell structurally maintains the multi-layered shielding and the cavity with appropriate support structure and also separates the cryostat vacuum from the exterior. The cavity, helium vessel and cryostat should be designed to withstand the maximum pressure taking into account the entire cooling cycle and the respective material properties. Appropriate relief valves on the cryostat and Helium vessel should be designed in case of a sudden pressure release to ensure the safe evacuation and maintain the integrity of the cryostat. The pressure conditions for SM18 and SPS test environment are summarised in the Table 4.

Table 4: Pressure conditions for the SM18 and SPS test environment.

Test environment	Safety valve (set-point)	Maximum allowable pressure (PS)	Test pressure (1.43xPS)
SM18 Test cryostat	1.5 bar±0.15*(abs)	1.5 bar (abs)	2.1 bar (abs)
SPS	1.8 bar±0.15* (abs)	1.8 bar (abs)	2.6 bar (abs)

In particular, the cavities that will undergo SPS tests have to be designed for a maximum external pressure of 2.6 bar. The corresponding helium tank has to be designed for a maximum internal pressure of 2.6 bar. The complete cryomodule assembly: cavity(ies), helium tank(s), vacuum vessel have to be treated for the same risk category as the most critical one. From the figure above assessing the risk category, a pressure vessel has to be treated as risk category *I* if the (maximum allowable pressure · fluid volume) is greater than 50 bar · litre and smaller than 200 bar litre. In particular, for a maximum allowable pressure of 1.8 bar, a helium tank enclosing a volume of 30 litre of helium has to be treated as risk category *I*.

4   FREQUENCY TUNING

The obtained resonant frequency of the RF cavity will depend mainly on the geometry or shape of the cavity and the change of that shape during cool down. Material properties such as the RRR of the Niobium will have a much smaller influence on the frequency.

Geometrical variations due to the forming, welding and surface treatments made during the fabrication of the cavity will result in a first frequency uncertainty on the bare cavity. The assembly of the cavity in the helium vessel to form the "dressed cavity", followed by the assembly in the cryostat can again alter the frequency. Stringent but realistic tolerances are defined on the fabrication of the cavity to limit the uncertainties of the frequency of the finished dressed cavity. Close follow up during the fabrication of the prototypes should improve the remaining uncertainty on the frequency.

4.1   REQUIREMENTS/ BOUNDARY CONDITIONS

The HL-LHC crab cavities should provide the deflecting field on the particle bunches at a frequency of 400.79 MHz, a frequency fixed by LHC operation parameters. The resonant RF frequency of the cavity should precisely fit to this operating frequency with a resolution at the level of 100 Hz in order to minimize the RF power needed to run the cavities.

The cool-down to 2 K will shift the frequency of the cavity by hundreds of kHz due to the thermal contraction of the components. During RF operation of the cavity, Lorentz forces will detune the cavity (Lorentz Force Detuning LFD) in the <1 kHz range. The frequency change during the cool down was modelled and will be anticipated on the target frequency at room temperature, after fabrication and surface treatment. Measurement of the frequency shift on prototype cavities should reduce the uncertainties during the series production.

Nevertheless, a tuning system to mechanically adjust the geometry and hence the frequency of the cavities during operation will be required with a range as large as possible. In addition, this tuning system is also required to move the resonant RF frequency of the cavity sufficiently away from the 400 MHz when the crab cavities are not used but when a particle beam is present. These frequency adjustments are in the first place slow quasi static processes with a resolution as mentioned above. Dynamic effects such as LFD and pressure variations will call for faster and precise adjustments that require small backlash and hysteresis.

This precision requirement in addition to reliability and maintainability considerations resulted in the choice of placing all moving and frictional parts of the motorisation outside of the cryostat, at warm and not in vacuum. The design of the motorisation should allow as much as possible for the possibility to exchange in case of failure.

Taking into account the available space for the cryomodule in the LHC tunnel, the best chance for an integration of an external motorisation is on top or to a smaller extend under the cryo-module. The motorisation on top must be integrated next to the RF wave guide, the coupler and the cryogenic jumper connection.

An operational requirement for the tuning is its compatibility with the alignment of the cavities in the accelerator. The tuning forces should not move the cavity from the aligned position by more than some tenths of a millimetre.

Finally, the presence of radiation should be taken into account. The components sensitive to radiation should therefore be accessible for preventive maintenance. In particular the lubrication, instrumentation and plastic components should be properly considered.

4.2   TUNER CONCEPT

In order to determine the tuning principle, the different frequency sensitivities by deforming different parts of the cavities such as the waist, centre plates and cavity length are calculated. The elastic range of each deformation gives the tuning frequency range reachable with that deformation. The final choice of the tuning principle is based on the range available, the space available in and around the cryomodule, required forces and their effect on the alignment of the centre of the cavity in order to avoid an offset during the tuning.

Advantageously, for both DQW and RFD, the selected tuning principle is the symmetrical displacement between two plates of the cavity, in the vertical direction. For the DQW (Figure 9) the distance between the central capacitive plates is symmetrical changed with a tuning sensitivity of 186 kHz/mm measured between the two plates. For the RFD the tuner deforms the outside horizontal plates symmetrically with a sensitivity of 345 kHz/mm, again measured between the plates.
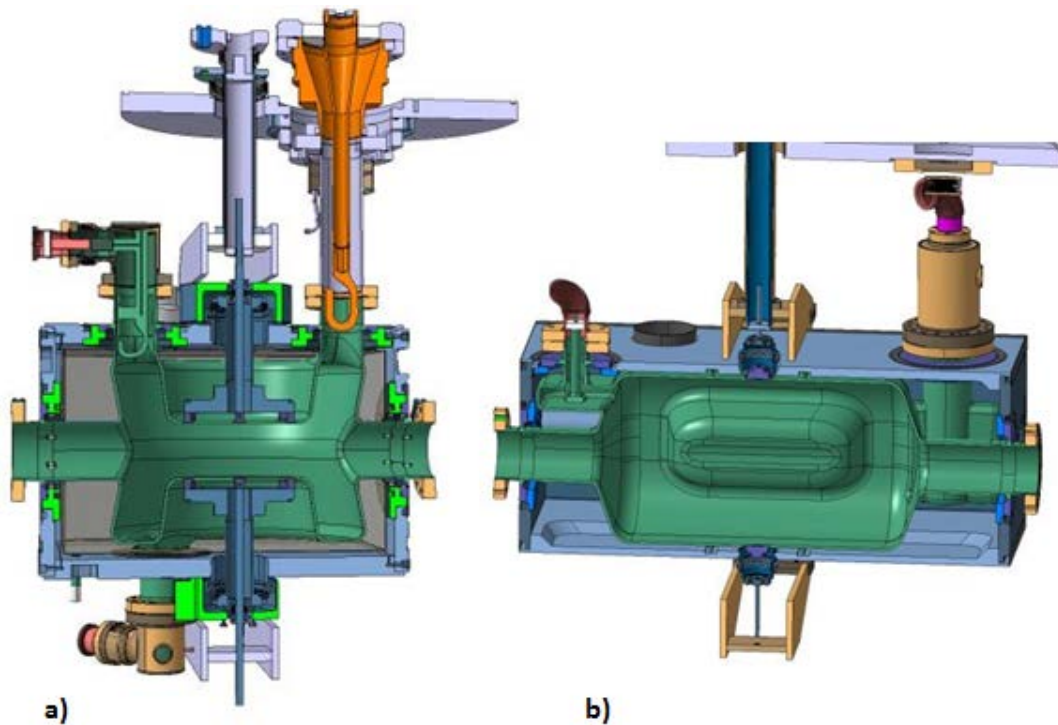
Figure 9: a) DQW and b) RFD tuning principle

With the selected solution, the motorisation (see below) is placed outside, at warm and at atmospheric pressure, easily accessible on top of the cryomodule. The motorisation induces a relative motion between two thin walled concentric tubes. This solution is based on an existing JLab design for CEBAF. The inner tube is connected through a helium tight bellow on the helium vessel to the top part of the cavity, the outer one is connected to a titanium frame that surrounds the dressed cavity. The bottom part of the cavity is connected to this frame. The mechanical connections of the tuner to the cavity walls are made with NbTi parts that are electron beam welded to the Niobium walls of the cavity. A relative displacement between the two tubes will hence create a symmetric deformation of the cavity.

A finite element analysis is made to evaluate the stresses and forces induced by deforming the cavity and for estimating the possible tuning range for DQW (Figure 10) and RFD (Figure 11). With the elastic limit of Nb at 2 K (400 MPa) and a safety factor 1.2, a range of ± 0.31 MHz (± for push and pull) for a displacement of 1.7 mm between the plates was calculated for the DQW and ± 0.980 MHz for a displacement of 2.8 mm for the RFD. The tuner has to provide a tuning force of 2.2 kN/mm for the DQW cavity and 2.5 kN/mm for the RFD.
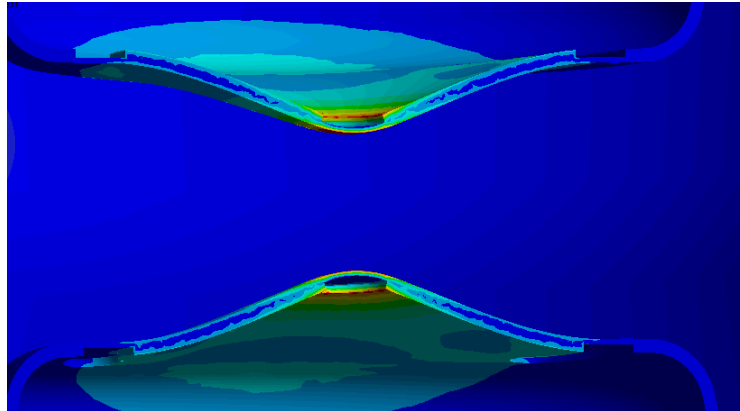
Figure 10: evaluation of the stresses and forces induced by deforming the DQW cavity in order to estimate the tuning range
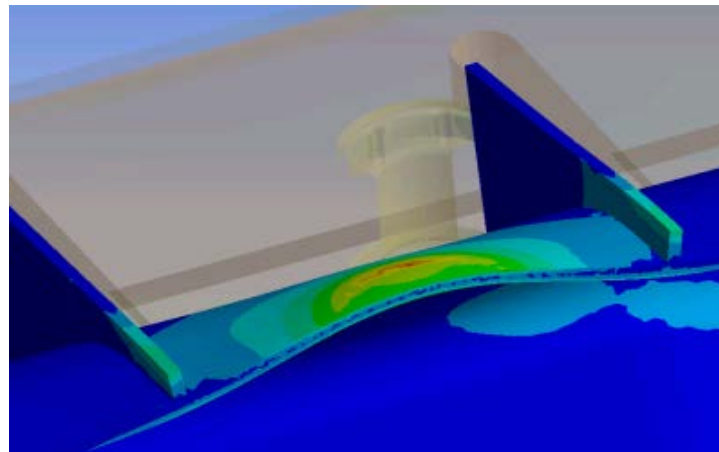

Figure 11: evaluation of the stresses and forces induced by deforming the RFD cavity in order to estimate the tuning range

The selected solution for the DQW results in a significantly lower tuning range compared to the RFD cavity. Therefore, a pre tuning feature is added to the DQW design, Figure 12 that can deform the cavity plates towards the outer radius by applying a load between the cavity and the helium vessel. Such a deformation is applied with screws at room temperature, after assembly of the dressed cavity. The frequency sensitivity of this deformation is 0.8023 MHz/mm (distance between plates), resulting in an additional ± 0.15 MHz elastic pre-tuning range and more if we allow plasticisation. As the resolution of this pre tuning with screws is limited, this is a coarse tuning method. The method requires the use of one additional helium tight bellow.
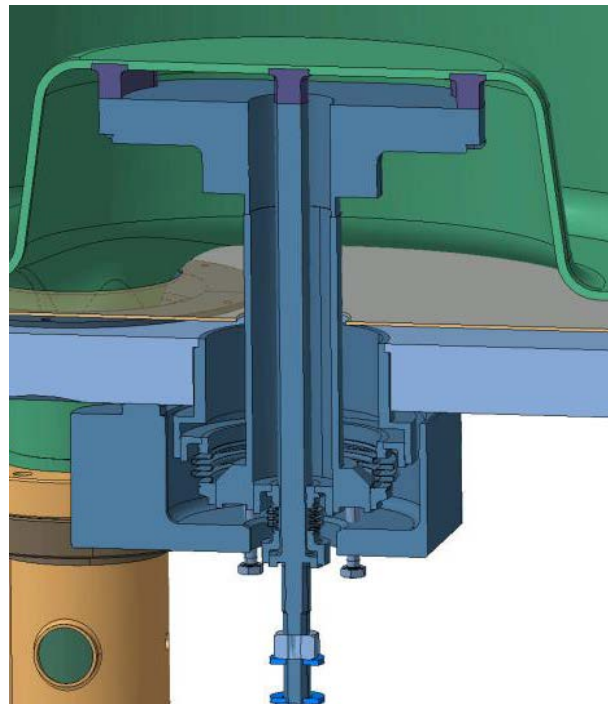
Figure 12: pretuning system in the DQW

4.3   TUNER MOTORISATION

The actuating system that displaces the concentric tubes is placed at room temperature and under atmospheric pressure. A stepper motor drives with a high resolution (1.8 deg/step) a harmonic gearbox with a 100:1 ratio. A roller screw, allowing smaller pitch (1 mm) compared to a ball screw with less friction, transforms the rotation in a linear motion, guided by linear roller bearings on precision guides. One motor step results in 0.1 µm resolution for the displacement between cavity plates i.e. a frequency resolution of 20 Hz for DQW and 35 Hz on the RFD. The resolution can be increased by dividing a motor-step or micro stepping, finally limited by the precision of the harmonic gear 0.1 arcminutes corresponding to 10 nm or 2 Hz for the DQW and 3.5 Hz for the RFD. The final resolution will however depend on the friction in the ball bearings and on the proper alignment of the components and shall be tested.

A first prototype motorisation was built (Figure 13) for testing the frequency tuning on the first proof-of-principle cavities in a test station. The motor has been assembled and at the time of writing tests are about to start.
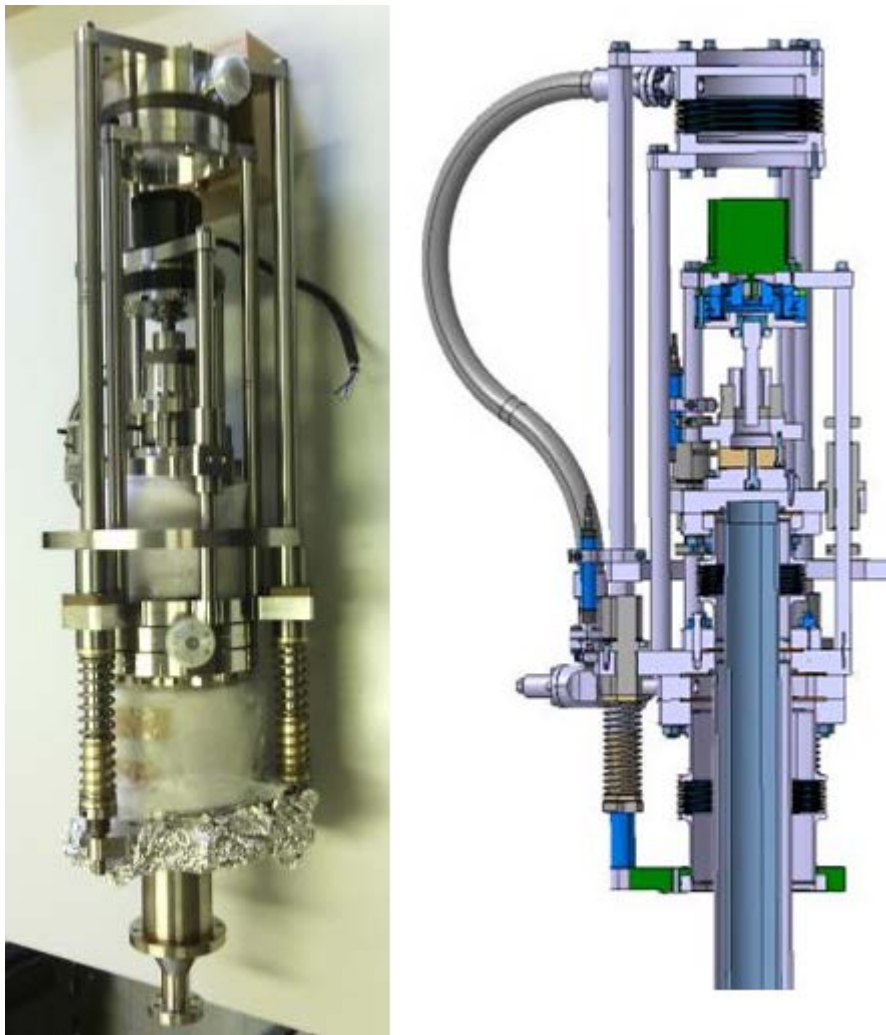
Figure 13: Prototype tuner motorisation

A pressure compensation feature was added to the motorisation. The vacuum in the cryo-module exerts a non-negligible force on the section of the tuner motorisation that cannot be transferred to the vacuum tank. In order to produce a symmetric displacement between the concentric tubes, the motorisation should be floating. It is therefore supported by mass compensating springs visible on Figure 13. Without pressure compensation the vacuum force would pull down the motorisation, creating a downward force on the cavity, changing its frequency and alignment. A pressure compensating bellow was therefore added in the motorisation to make it less sensitive to vacuum or atmospheric pressure changes.

In this vertical design, with the current components, the limit force capacity is set by the harmonic gear box at 7.7 kN dynamic force, compatible with the values mentioned above. The stepper motor has sufficient torque and the detend torque is sufficient to make the motorisation self-locking.

The vertical size of the built prototype is too large for integration under the RF guide. A design optimisation is therefore ongoing to reduce that dimension (Figure 14). This design can also be completely dismounted from the cryomodule without opening the vacuum vessel. Finally, a horizontal design is under study in order to increase the very small clearance to the RF guide

for the vertical design. This horizontal design introduces, in addition, a way to increase the resolution of the tuner further.
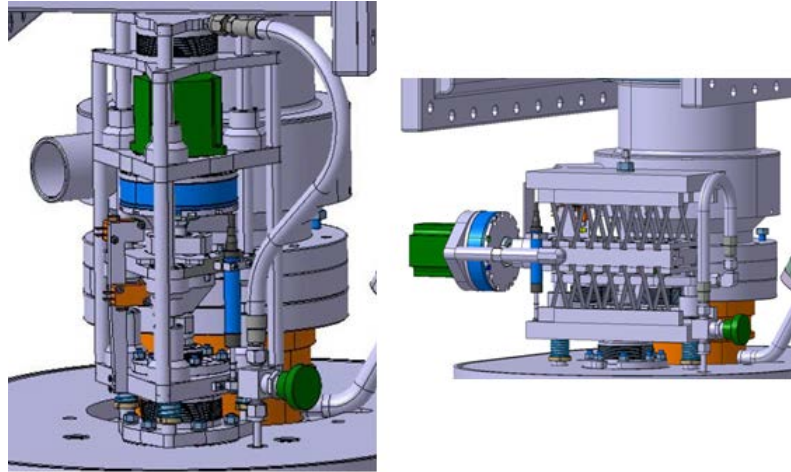

Figure 14: a) Vertical design with reduced size b) horizontal design with increased resolution

5   STRENGTH ASSESSMENT OF THE DRESSED CAVITIES

The next sections will provide an overview of the strength assessment of the He tank. The He tank is subjected to a pressure of about 1.8 bar during cool-down. Therefore, it acts as a pressure vessel and requires careful evaluation of its strength. The analysis of the bare cavity is also going to be reviewed, as its performance strongly depends on the tank.

5.1   OVERVIEW OF THE HELIUM TANK

The helium tank will contain saturated superfluid helium at 2 K, cooling the cavity and allowing the extraction of the heat dissipated in the cavity and adjacent cold components. Superfluid helium is an excellent thermal conductor for small heat flux. Above a critical heat flux, the temperature increases drastically and eventually superfluidity is lost. The geometry of the helium tank has been determined to allow this maximum heat extraction while optimising the quantity of the helium to be used.

Two choices of material have been studied for the helium tank: stainless steel and titanium. The titanium has the advantage of roughly the same thermal contraction as niobium (in the order of 1.5 mm/m from ambient temperature to 2 K), while the thermal contraction of stainless steel is twice as large leading to larger thermal stresses. The advantage of stainless steel is the manufacturability and thus the cost. However, for the unconventional geometries of the crab cavities, titanium grade 2 was chosen as the optimum material for the helium tank, allowing for rigid connections of cavity ports to the helium vessel.

The helium tank has a structural role and its rigid connection to the cavity ports ensures optimum boundary conditions for the cavity during mechanical loading, in particular during maximum pressure loading and tuning. The helium tank geometry was chosen to limit the maximum stress on the cavity to tolerable values [13]. In facts, the stress distribution in the cavity, as well as the maximum values, is directly influenced not only by the cavity geometry but also by the helium tank configuration.

The initial design based on a fully welded helium vessel has been discarded due to high deformations occurring after welding. It has been estimated -see Figure 15 for test pieces- that a 3 mm weld seam would determine a 1 mm deformation at the interface with the cavity. On top of that the quality of the welds is not optimal. The bolted helium vessel with additional leak-proof welds emerged then as design concept.
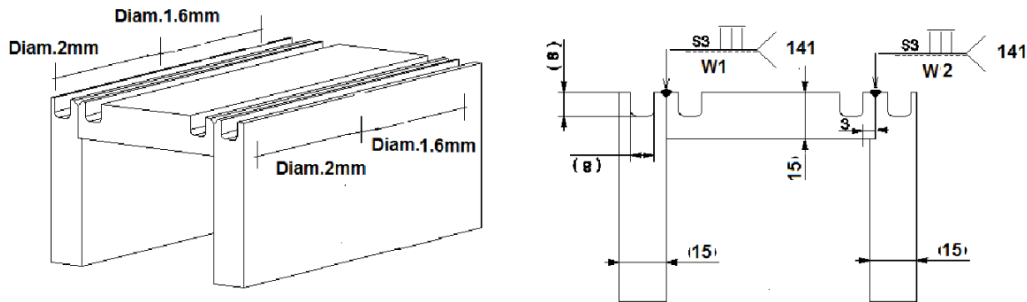

Figure 15: Test structure for evaluating the deformations after welding

As there is no experience with such approach at CERN (and worldwide it's an uncommon design), the calculations are performed for the worst-case scenario. It is assumed that there is no friction between the tank plates and the full load is carried by the bolted joints and leak-proof welds. The bolt behaviour is examined using ANSYS. Reaction forces and moments are estimated from the numerical calculations and used to perform calculations for the bolted and welded joints. The final assessment of the helium vessel includes the verification of the bare cavity along with all the bolts and welds.
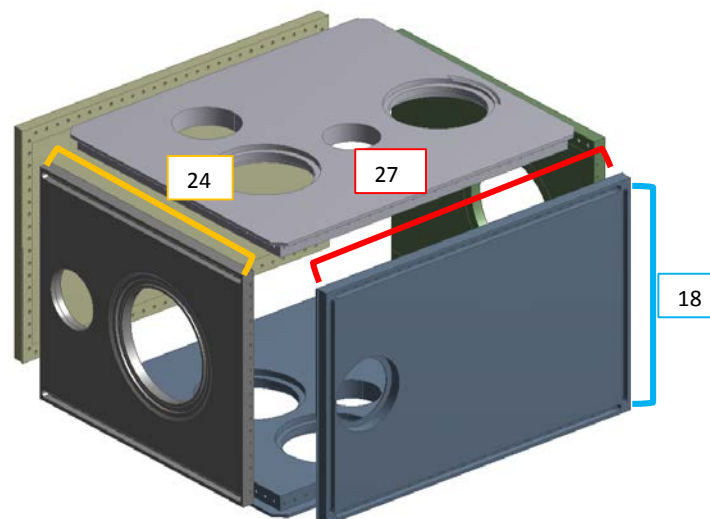

Figure 16: DQW helium vessel with the bolt location.

5.2 MAIN LOADS CONSIDERED

The results reported here are obtained from what is considered the worst load case shown in Table 5. The calculations are made at room temperature mainly due to the low yield strength of niobium. Indeed, all the load cases of the tank/cavity system are evaluated.

Table 5: Loads considered for the He-vessel mechanical calculations..

T = 300 K	Load	Bolt pretension	Gravity	Pressure	Pre-tuning
	Value	4500 N	9806.6 mm/s2	0.18 MPa	0.2 mm

Independent steps are defined in ANSYS to facilitate checks and comparison for any of the loads, however the final assessment is performed on the combined load.

5.3 ASSUMPTIONS AND BOLT MODEL

Helium vessel plates are fastened using the bolt joints evenly distributed along 12 edges (Figure 17). Identical tapped bolts are placed in grooves with the same spacing for the same grooves.
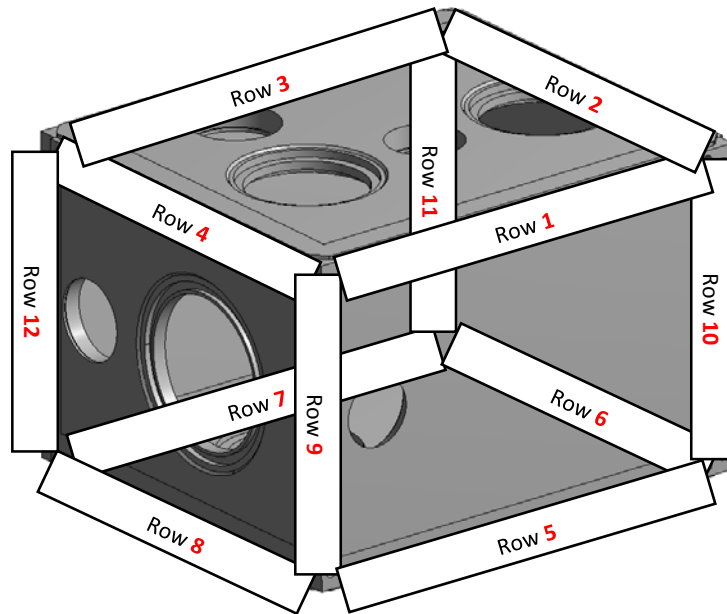
Figure 17: DQW helium vessel with position of bolt rows.

Three configurations of the plate connections are depicted in Figure 6 (Table 6 for the configuration of each row). The variants a) and b) are the same except for the chamfer. They are used for the top and bottom cover plates and the design c) is employed for the sides. Different designs of the connections are imposed by the assembly requirements and result in different performance of the bolts.
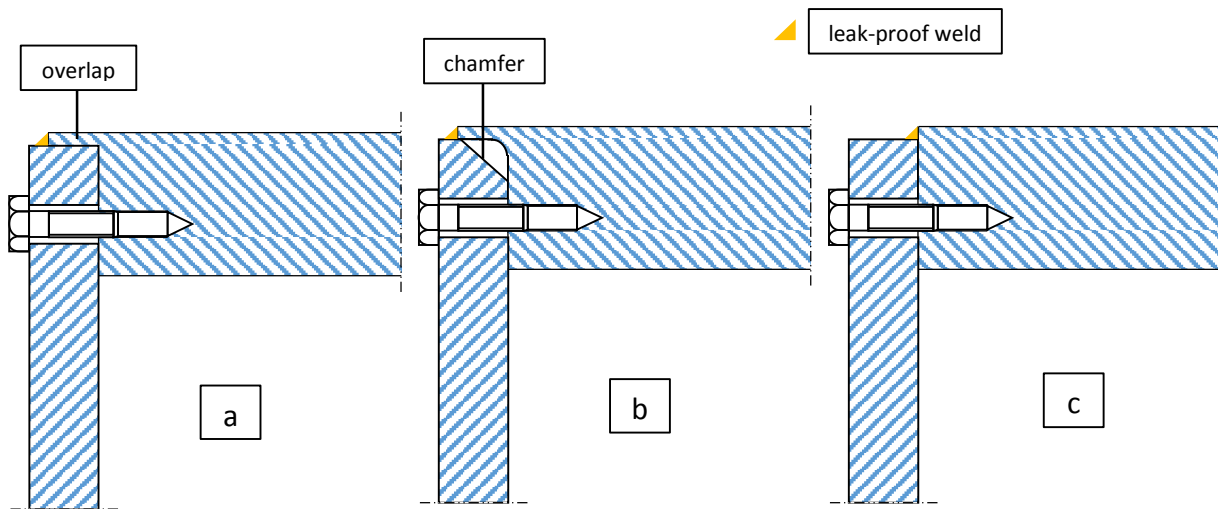
Figure 18: Three different types of the plate connections.

Table 6: Assignment of the connection type to the bolt row.

Configuration	Row
a	1, 3, 5, 7
b	2, 4, 6, 8
c	9, 10, 11, 12

The bolts are modelled in ANSYS (Figure 19) according to VDI 2230:2 [16]. Titanium grade 5 is selected as a bolt material, because of its high proof stress and coefficient of thermal expansion almost identical to titanium grade 2. The bolts are modelled as beam lines with cross section properties calculated using VDI 2230:1 [17] procedures. The bolt length is represented as the shank length between the bolt head and the threaded hole. The beam top and bottom nodes are coupled with the projected head face and threaded hole to simulate a fixed beam. The bolt preload is chosen arbitrary as a consequence of lack of codes fully applicable to this case. The main requirement is to avoid the joint separation in condition of zero contact pressure between the plates.

The loads experienced by the bolts include: the axial tensile force, the transverse shear force, the bending moment and the torsional moment due to wrenching. In order to calculate the highest stress the combination of those forces/moments is combined and compared with the allowable value. The axial tensile force consists of the preload and the applied load component that also includes the prying force. That force is generated as a result of the local rotation of the cover plates around the edge under an applied pressure. The shear force is an outcome of the relative movement of the plates that in parallel generates a bending moment. The prying force effects in increasing the bending moment especially in the midpoint of the grooves, where the plate rotation angle is the highest. The torsional moment is a residual moment due to the preloading bolts using a wrenching torque.

The maximum values of the loads in the bolts are shown in Table 7 and are extracted from two different models. The first one constraints the plates only with the bolts, therefore neglecting

the effect of the welds. The second one has both bolts and welds, instead. This allows checking the safety coefficients for the stand-alone performance of the bolts along with the effect of the weld joints.
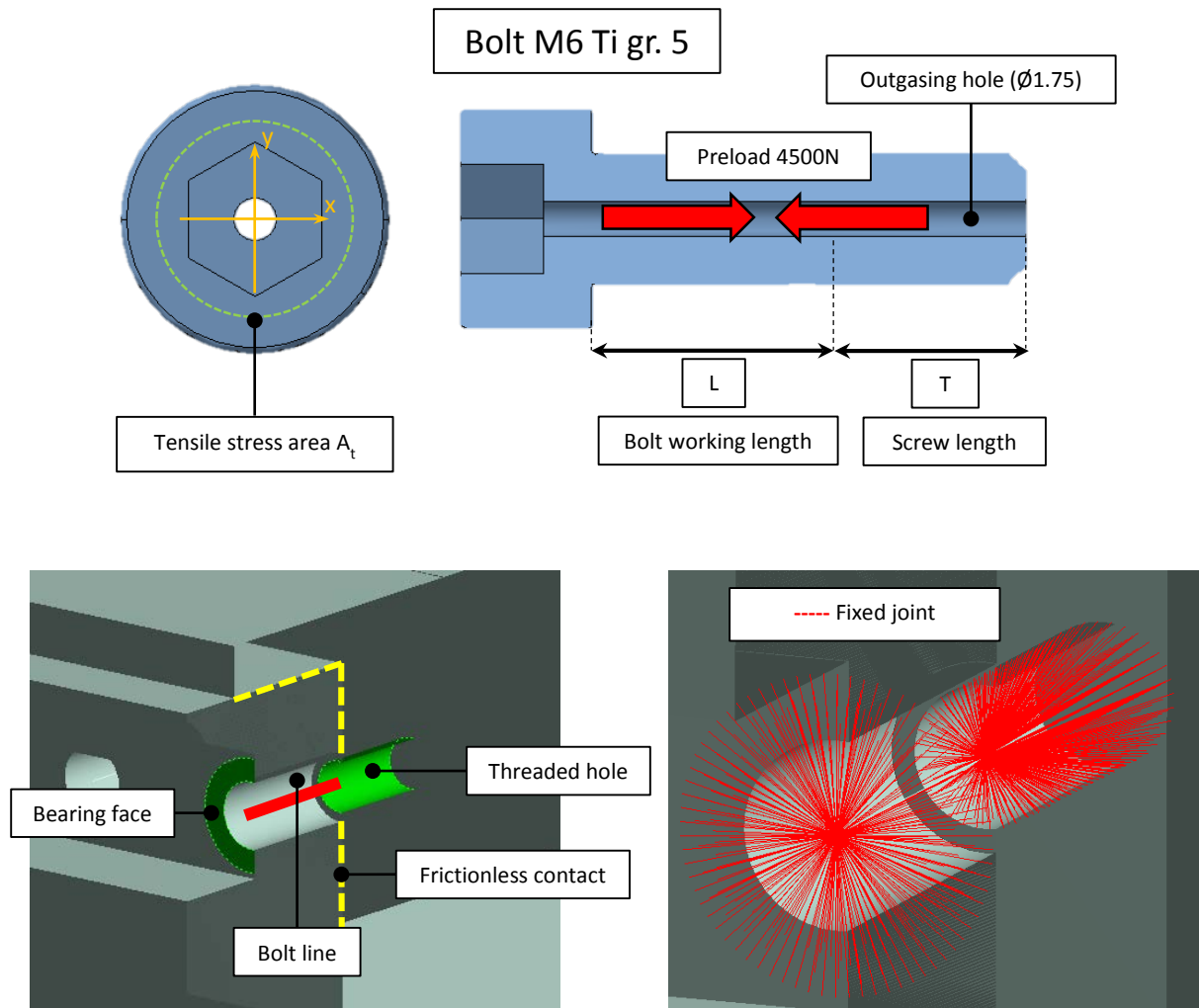

Figure 19: Bolt modelling in ANSYS.

The calculations show that the bending moments and shear forces heavily contribute to the high stress level of the bolts. It is worth reminding that friction between plates, whose value is highly uncertain, is here neglected. According to these analyses, the safety coefficient is acceptable in these conditions even following a worst-case approach.

Table 7: Results for the bolts.

Name	Symbol	Unit	Case	
			Bolts	Bolts + welds
Preload	P	[N]	4500	
Max. axial force	F_A	[N]	4650	4655
Max. bending moment	M_b	[Nmm]	3430	1630
Max. shear force	T	[N]	525	245
Equivalent stress	σ_{eq}	[MPa]	620	480
Proof stress Ti gr. 5	S_p	[MPa]	830	
Safety factor	k	-	1.34	1.74

5.4 WELDS MODEL AND ASSESSMENT

The weld seams encompass the cover plates in parallel to the bolt rows and provide the leak tightness of the vessel. Although the function of the welds is not structural, the reaction moments and forces are carried in part by them and a strength assessment is required to check their performance. The calculations are based on the assumption of a uniform distribution of the loads through the weld length. The welds are treated as lines and divided into two groups (Figure 20):
   1. Bottom and top welds with a rectangular profile
   2. Downstream and upstream welds with a profile made of two parallel vertical lines

Table 8: Properties of the weld group [Ref: 19].

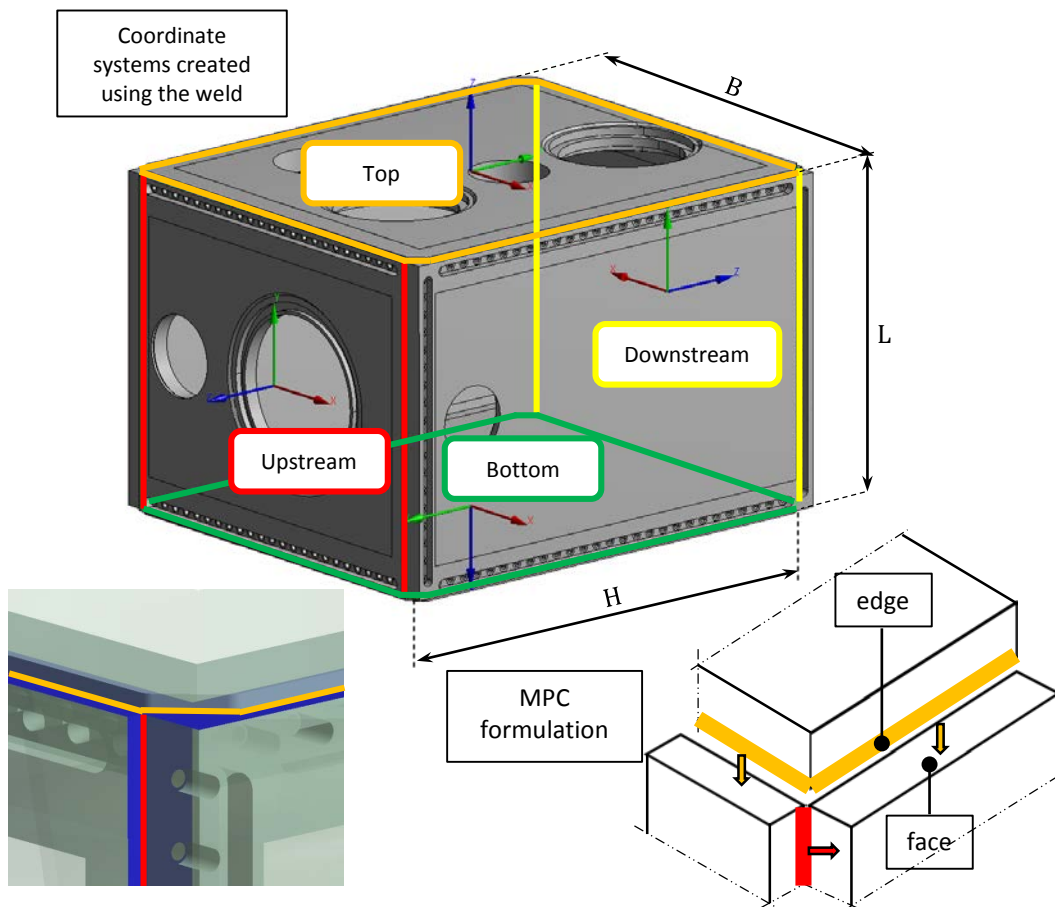| Shape	A [mm^2]	I_x [mm^4]	I_y [mm^4]
||	$2aL$	$\dfrac{aL^3}{6}$	$\dfrac{L((B+2a)^3 - B^3)}{12}$
▢	$2a(H+B)$	$\dfrac{aH^3}{6} + \dfrac{B((H+2a)^3 - H^3)}{12}$	$\dfrac{aB^3}{6} + \dfrac{H((B+2a)^3 - B^3)}{12}$

Figure 20: Weld modelling in ANSYS.

The weld group properties are calculated with the throat thickness a = 1.5 mm and with the weld section properties in Table 8. The leak-proof welds are modelled as edge-to-face bonded contacts with the MPC (multipoint constraint) formulations. In the FE analysis, the welds are defined after the bolt preload not to pre-stress them. In order to obtain the reaction components relative to the weld centroid, the corresponding coordinate systems are created. The reaction forces/moments are subsequently used to calculate the equivalent stress.

The combined stress is an average value, whereas he peak stress can be significantly higher. However, the peak would be localized and is taken into account only in case of fatigue, which is not an issue for the Helium tank. Thus, keeping in mind that the proof stress for Ti gr.2 is 280 MPa, the results show in Table 9 validate the welds and ensure their structural integrity.

Table 9: Example of extracted reaction forces/moments with the equivalent stress.

Welds	F_x	F_y	F_z	M_x	M_y	M_z	σ_{eq}
	[N]			[N·mm]			[MPa]
Top	-504	1873	-15962	19652	-325050	164750	9.02
Bottom	522	1253	-15946	430170	-283260	339480	9.90
Upstream	-1406	-1980	6895	-61508	248090	63502	12.87
Downstream	-47	-926	7517	-54226	-323140	-14590	12.88

5.5   HELIUM VESSEL ASSESSMENT

The helium vessel is assessed checking the stress level and the total deformation. The stress is examined overall using the full model and also for three cutting planes to extract the values inside the plates (Figure 21). The highest stress occurs in a localized region close to the bolt head (Figure 22) this peak is due to numerical effects generated by the presence of the sharp edge and is not considered in the overall assessment. Everywhere else the stress is low. The total deformation presented in Figure 22 is small and do not affect the structural performance of the vessel. The final tank will present some slots machined into the plates in order to reduce the total mass. The size of these features, however, has been chosen such that no change is observed in the stress in tank and cavity. For this last vessel the results are then almost the same. The calculations show that the helium vessel design can be fully accepted.
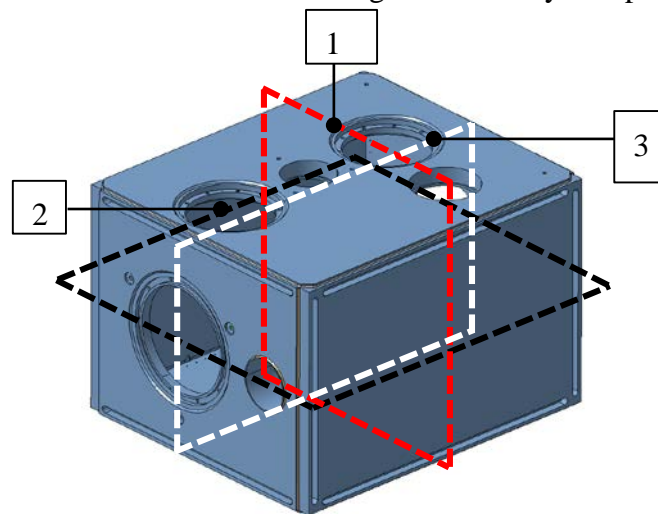

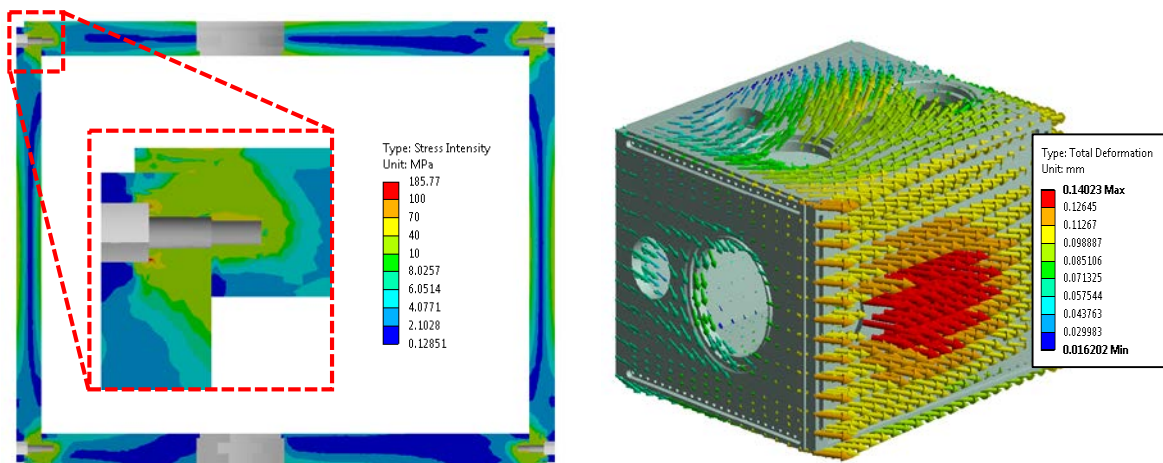*Figure 21: Cutting planes for the helium vessel.*

Figure 22: Stress intensity for the cutting plane #1 (left), DQW helium vessel total deformation (right).

5.6   CRAB CAVITY ASSESSMENT

The bare cavity is assessed according to EN13445-3 [18]. A sub-model procedure is required for limiting the number of elements in the full model. This sub-model is created by cutting the cavity from the global model and importing the displacements for the sections underlined in Figure 21. It provides higher resolution and detailed information about the stress level. The analysis shows locations where the stress level is above the Nb proof stress (75 MPa), as shown in Figure 24. Therefore the analysis was detailed according to "Design by Analysis - method based on stress categories" from EN13445-3. The effect of the different loads has been differentiated: gravity and pressure generate primary stress in the cavity while pre-tuning effect generates secondary effect (the basic characteristic of a secondary stress is that it is self-limiting). The classification of the stresses into membrane and membrane + bending is made using the supporting line segments passing through the cavity thickness in some particular spot. Therefore, for each relevant spot membrane (P_m), bending (P_b), primary (P) and secondary (Q) stresses have been evaluated. The results in Table 10 for all the considered locations comply with EN13445-3 and confirm that the values of the stress for the cavity are acceptable. The analysis for the spot 8 was not performed since the stress level is due to a geometric singularity and the maximum stress is mesh dependant.
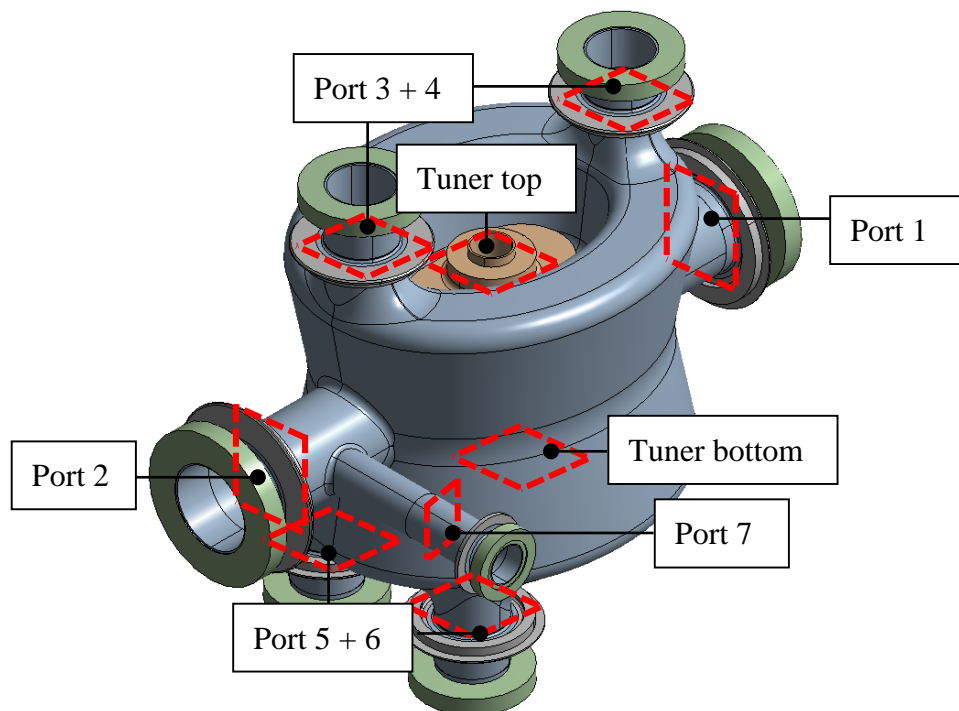
Figure 23: DQW crab cavity with the cutting boundaries.
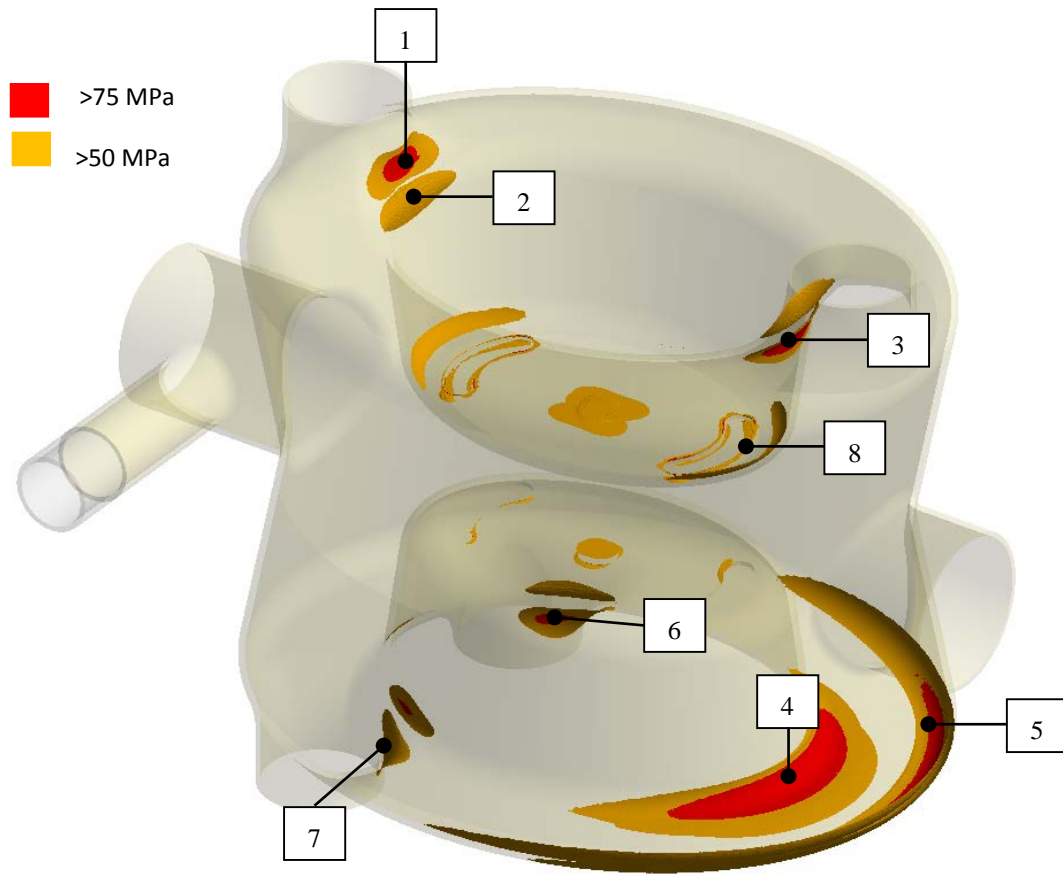
Figure 24: DQW crab cavity with the stress classification lines.

Table 10: Stress assessment according to EN13445-3.

Classification line	Stress category	Allowable stress [MPa]		Calculated stress [MPa]
1	P_m	f	50	27
	$P_m + P_b$	1.5f	75	55
	$\Delta(P+Q)$	3f	150	110
2	P_m	f	50	17
	$P_m + P_b$	1.5f	75	58
	$\Delta(P+Q)$	3f	150	110
3	P_m	f	50	15
	$P_m + P_b$	1.5f	75	59
	$\Delta(P+Q)$	3f	150	112
4	P_m	f	50	7
	$P_m + P_b$	1.5f	75	58
	$\Delta(P+Q)$	3f	150	121

5	P_m	f	50	10
	$P_m + P_b$	1.5f	75	44
	$\Delta(P+Q)$	3f	150	74
6	P_m	f	50	29
	$P_m + P_b$	1.5f	75	54
	$\Delta(P+Q)$	3f	150	54
7	P_m	f	50	15
	$P_m + P_b$	1.5f	75	45
	$\Delta(P+Q)$	3f	150	83

6   ALIGNMENT MONITORING SYSTEM AND CAVITY POSITIONING

6.1   CAVITY SUPPORT CONCEPT

Before operation, the orientation and position of the cavity is adjusted by means of a plate rigidly connected to the dressed cavity. Such a plate is supported iso-statically in 3 points (Figure 25). Its position and attitude can be modified by setting the position of these 3 support points.
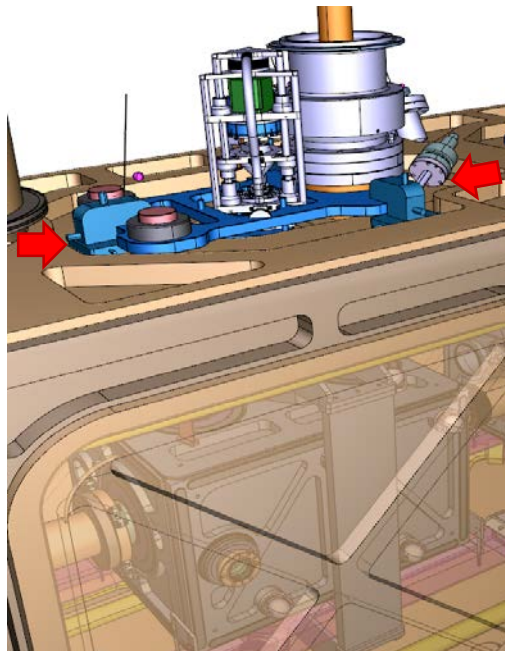

Figure 25: alignment plate (blue) with the supports used for attitude and position actuation. Two of them are visible and highlighted with the red arrows.

The rigid connection between the cavity and the alignment plate is obtained by means of the FP RF coupler and a set of additional supports. Several designs for these additional supports are

considered and analysed. A simplified version of the RFD dressed cavity is used for this comparison. This has the same approximate mass but a simplified geometry allowing for an increased efficiency in analysis. The main alternative concepts can be found in Figure 26.
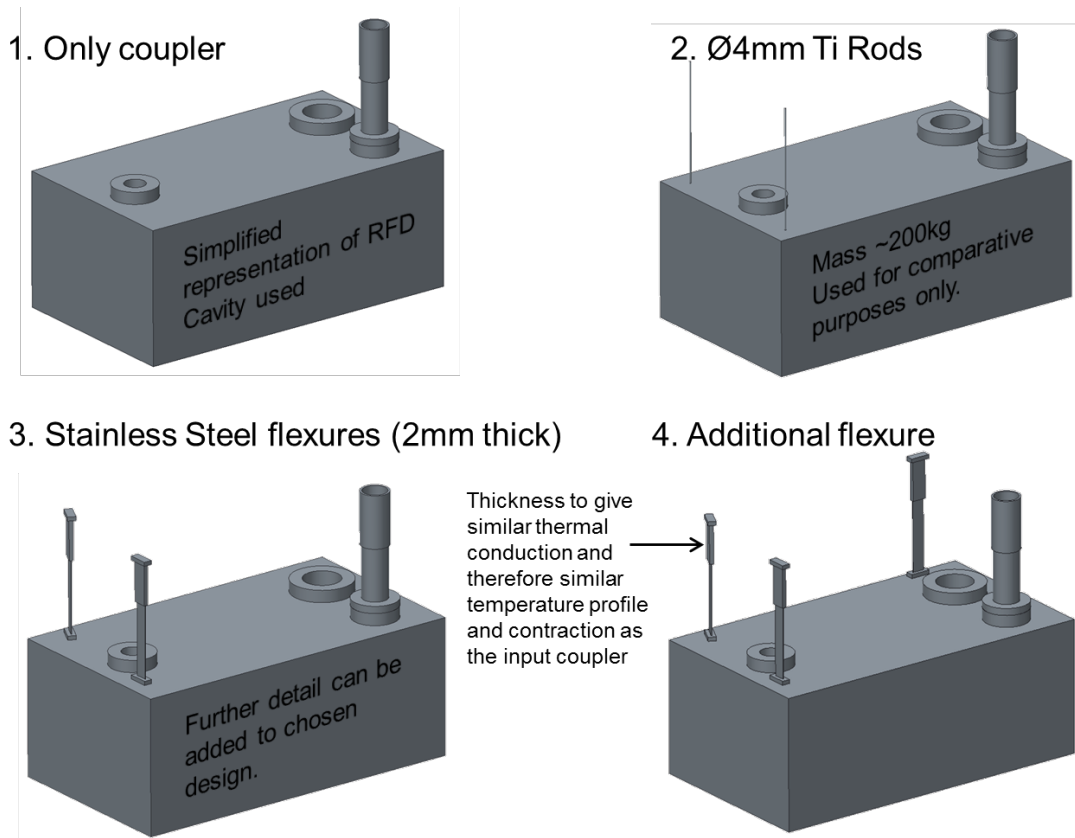

Figure 26: Support options considered for SPS Compact Crab Cavities

The cavities are analysed for self-weight deflection and stress, and the first 4 modes of vibration found for each. Table 11 shows the results of these calculations. The performance of the supporting system is significantly increased with a 'blade' type flexure arrangement. These give an increase in overall stiffness whilst still allowing for thermal contraction on cool down to 2K towards the fixed point, which is the input coupler. These cool-down deformations can be observed in Figure 27. The blade arrangement also has very few components. Further analyses are then performed to characterise the blade design. This is to give preliminary inputs in the design when considering integration issues. Both the distance from the coupler and the width of the blade are parameterised. Further analyses with detailed models of each cavity type are foreseen following the integration exercise. This will assess the final deformation expected as well as tuning vibration modes to ensure excitation of the cavities is minimised.

Table 11: summary of mechanical performance of the 4 concepts analysed for the supports

Analysis	Max Deformation [mm]	Max von-Mises Stress [MPa]	Mode 1 [Hz]	Mode 2 [Hz]	Mode 3 [Hz]	Mode 4 [Hz]
1	3.9	183	7.7	8.3	16.1	61.1
2	0.24	65.2	8.5	25.3	38.3	70.9
3	0.025	15.3	25.1	48.3	56.5	122
4	0.01	10.5	27.2	50.15	66.9	174
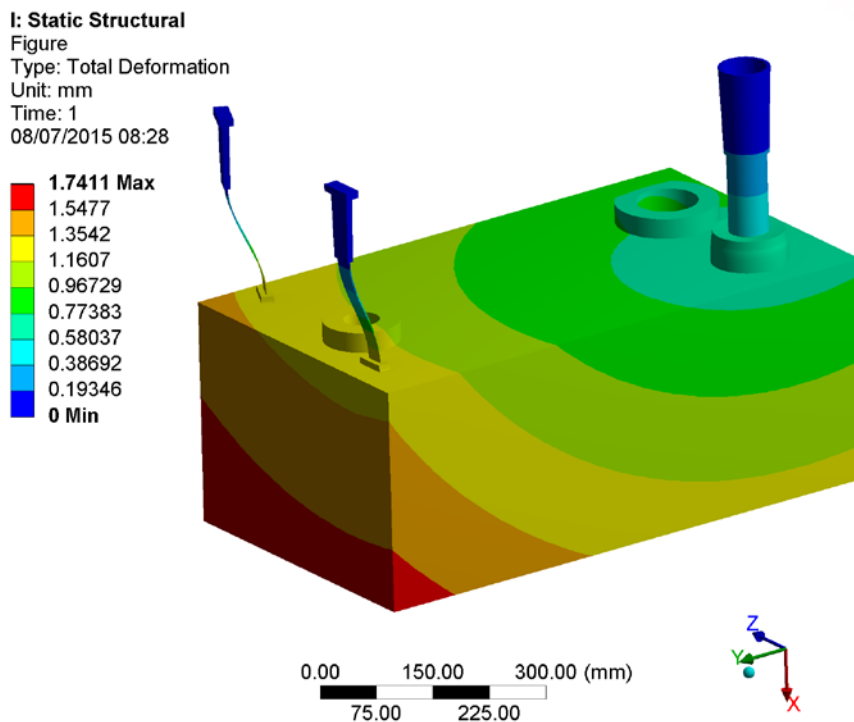
Figure 27: deformation of the support system during cool down.

6.2   ALIGNMENT REQUIREMENTS

Successful operation of the RF cavities depends on their correct position and attitude. The configuration constrains result from the transverse and longitudinal alignment tolerances described in the LHC performance requirements which primarily refer to alignment of individual cavities w.r.t to the beam [13]:

1. Cavity rotation in the X-Y plane (Rz, Figure 28) - it is required that the transverse rotation has to be < 0.3° (3σ) per cavity;
2. Cavity roll with respect to the cryostat axis should be less than 1 mrad (3σ), Figure 28;

3. Transverse displacement of cavities w.r.t each other inside a cryostat: intra-cavity alignment in the transverse plane with respect to the cryostat axis should not exceed the 0.5mm (3σ) tolerance set by the multipolar effects.

Figure 28: Crab-cavities alignment tolerances inside the cryostat
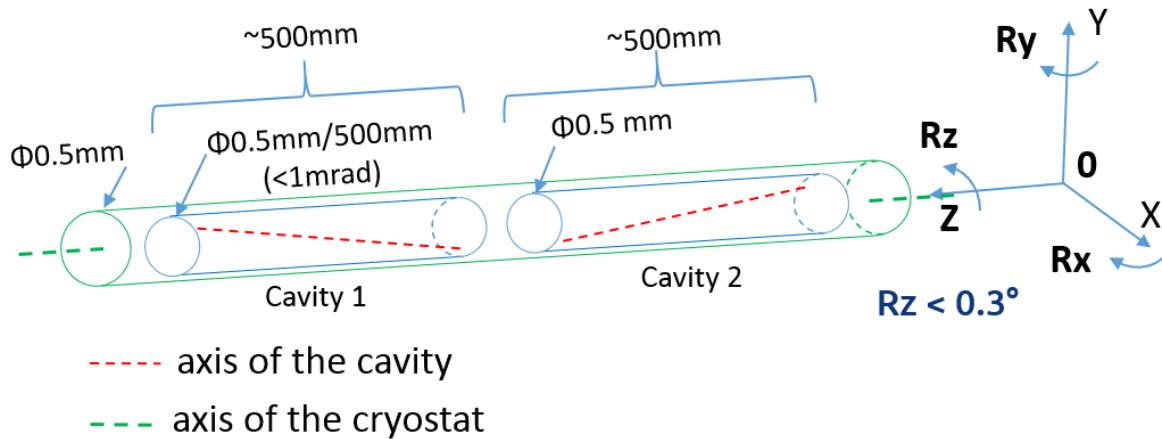
6.3   POSITION MONITORING GOAL AND PROPOSED SOLUTION

In order to monitor the alignment of the cavities w.r.t. given references at the accuracy level of 0.5 mm, the position monitoring system needs a sensitivity 5 to 10 times higher. Considering the need of alignment of the mean axis of the cavities within a 0.5 mm diameter cylinder, the precision or of the monitoring system has to be at the level of 50-100µm.

One of the challenges in creating such a system is the measurements of position of the cryogenic components from the warm cryostat (i.e. room temperature). Moreover the position of the referential frames of the cavities and cryostat has to be determined with respect to each other through absolute measurements. There are two main issues concerning cold objects measurements. The dressed cavities geometry can only be measured accurately by means of Coordinate Measurement Machines (CMM) at room temperature. After cool-down the geometry of components changes, so the CMM data will have to be corrected through models using the materials contraction coefficients. This is not trivial considering the nonlinear behaviour of the materials contraction coefficients with temperature and the complex design of the cavities. However, the use of Titanium, that has a contraction coefficient similar to Niobium, and the fact that the cavity is much less stiff than the tank should make the change in shape as linear as possible. The temperature gradient between the sensor head and the object may have impact on the result of the measured values. Therefore, non-contact methods are preferred.

The second challenge is that the cavities are located in a high radioactive environment. The components of the monitoring system will have to be radiation hard, keep stable properties over time along their whole work period and work without significant human interaction. Preliminary estimations of total ionising doses during HL-LHC operations due to the components installed close (5 cm) to the cavities show values as high as 10 MGy [20].

Assuming the conditions described above, the Frequency Scanning Interferometry (FSI, [21]) is chosen as a baseline solution. The FSI system offers absolute interferometric distance

measurement capability at sub-micron level. Only passive components (mirror, collimator, fibres) are needed at the points of measurement, which makes the application suitable for a high radiation level of operation.

In order to verify the performance of the FSI system during the preliminary prototype tests, a second solution based on the Brandeis CCD Angle Monitor (BCAM) is chosen [22]. The BCAM system is not radiation-hard and only allows to control the crab cavities position during the installation and preliminary tests.

6.3.1 FSI

FSI is a measurement technique that allows the determination of absolute distances with high accuracy. It determines the length between 0.2 m and 20 m with a measurement uncertainty (95%) of 0.5 μm/m. The FSI unit consists of a reference interferometer and a measurement interferometer that use tuneable lasers (from 1410 nm to 1510 nm). The length of the measurement interferometer (L_M) is expressed as a function of the reference interferometer length (L_R precisely known) and the ratio of phase change induced in the two interferometers is determined by frequency scanning [23]:
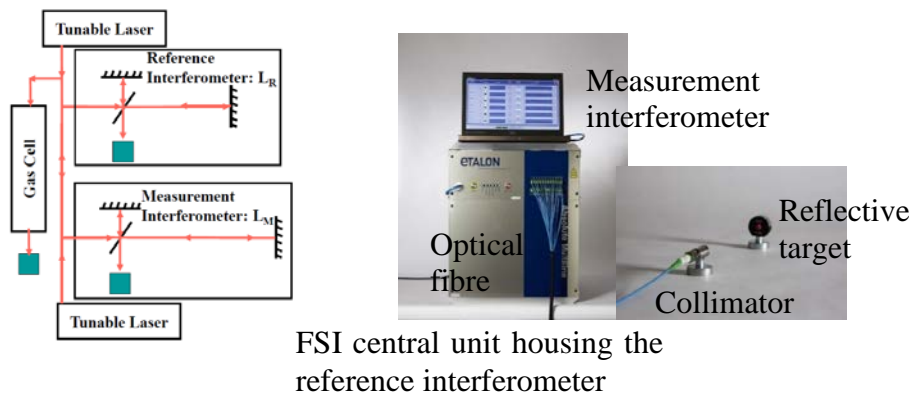
$$LM = LR \frac{\Delta\theta M}{\Delta\theta R}$$

Figure 20: Absolute interferometer: schematic (left), key elements (right) [27].

where $\Delta\Theta_M$ is the phase change in the measurement interferometer and $\Delta\Theta_R$ is the phase change in the reference interferometer. The schematic of the absolute interferometer is shown in Figure 30. The addition of a second laser tuned in opposite direction allows the removal of the drift error and the distinction between the phase changes caused by laser frequency variations and the phase changes from the optical path. The gas cell ensures stability of the reference interferometer.

In order to measure the position of the dressed cavities, several lengths between FSI system heads and reflective targets are measured (Figure 30). The position of the cavities can then be computed taking into account:

- the measured distances;
- the "known" geometry of the objects to be measured (depends strongly on the proper values of thermal contraction coefficient used for modelling of crab cavity dimensions

compensation when cool-down), e.g. the positions of the reference reflector targets w.r.t. cavity axis;

• the position of the measurement system components (FSI head positions within external coordinate systems)
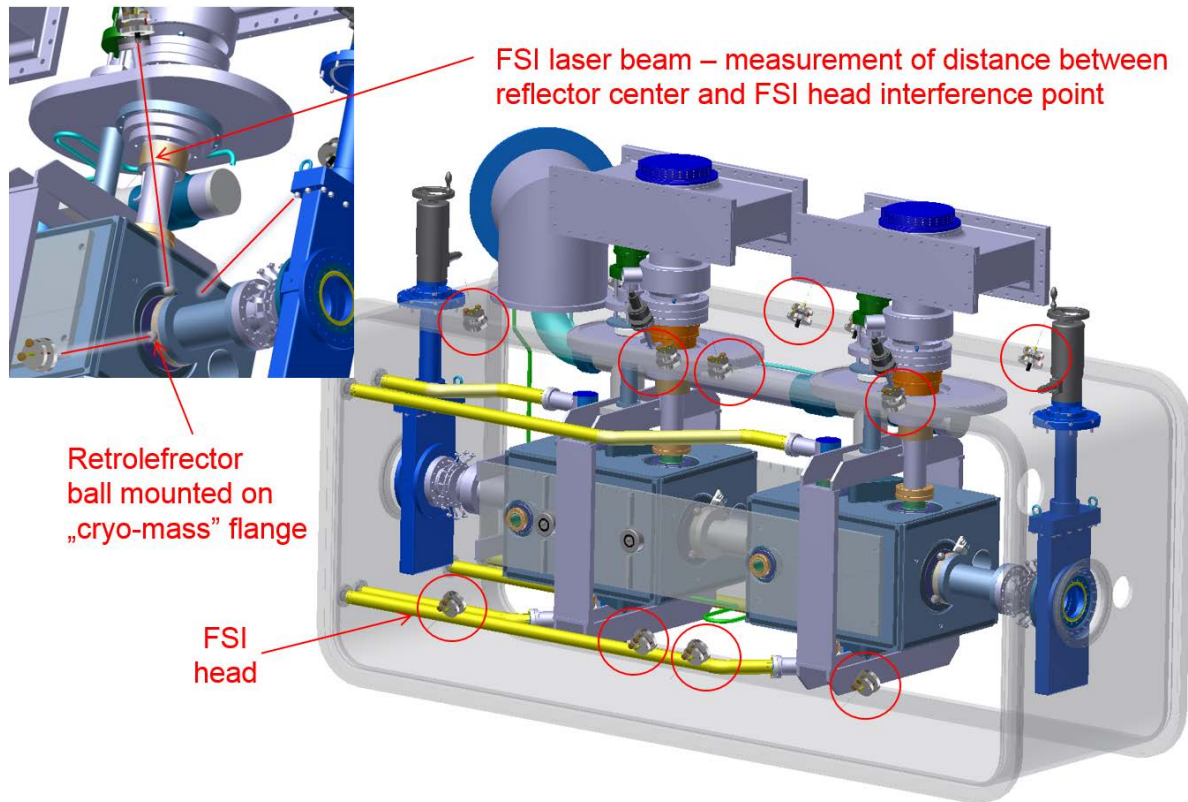

Figure 30: FSI system schematic for Helium Tanks of Crab-Cavities position measurements

6.3.2 BCAM

The BCAM system for crab-cavities is designed as a derivative of a similar solution developed for HIE Isolde cryostats [25].The basic concept is the creation of a closed geometrical network continuously monitored using a set of opto-electronic sensors linked to external references defined in the cryostat coordinate system (Figure 31). The positions of the cavities are measured in this geometrical frame. Double-sided Brandeis CCD Angle Monitor (BCAM, [22]) cameras installed on precise metrological tables on the cryostat sides look at each other and at four target "fingers" attached to the cavities (Fig 4). In such a way two external lines of sight are created, allowing the reconstruction of the position of the cavities.

The referential frame and the position of each active component is calculated from redundant observations using a specific 3D compensation software [26]. This measurement is performed taking into account BCAM to BCAM observations, image coordinates of the targets on the BCAMs, mechanical dimensions of supports and links, BCAMs calibration parameters, thermal effects and distortions of the optical ports located between atmosphere and high-vacuum.
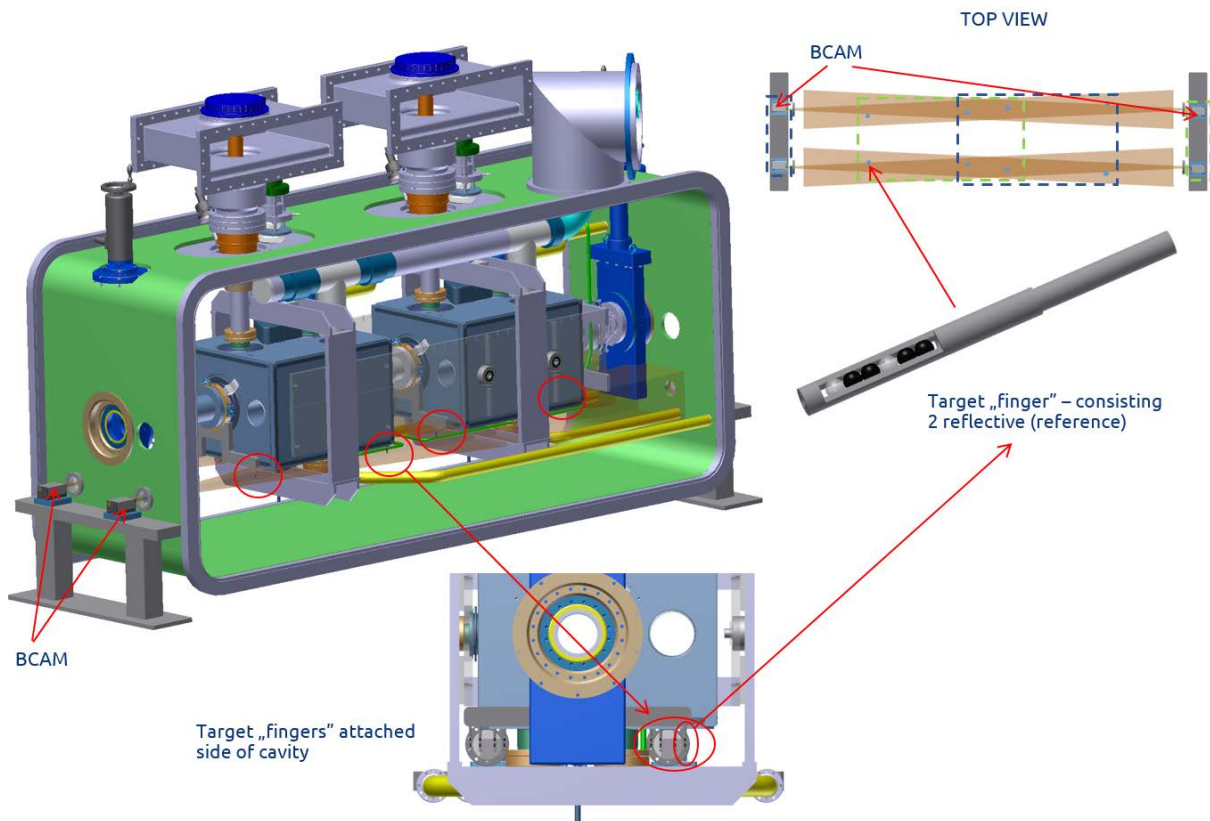
Figure 31: BCAM system schematic for Helium Tanks of Crab-Cavities position measurements

7   OPERATING TEMPERATURE & HEAT LOADS

The operating temperature of 2 K is chosen as a baseline for both the SPS tests and the final LHC installation [2]. In addition to the thermal margin available for machine protection and operational stability at 2K, the global availability of 2 K He is another important factor for the final operating temperature choice. At a nominal voltage of 3.4 MV, R_s of 10 nΩ and $RT.R_s = 3.7 \cdot 10^4$, the dynamic heat load per cavity due to the surface losses is ~3 W at 2 K. This leads to a manageable dynamic heat load of the final LHC system with 12 cavities per IR, even assuming a safety 50% safety factor on additional heat load. As the BCS resistance at 400 MHz and 2 K is ~1 nΩ, cavity surface resistance is primarily dominated by the residual resistance contribution, and any improvement in surface treatment should lead to lower surface resistances and hence reduce the dynamic heat load proportionally.

7.1   SPECIFIC CONSTRAINTS ON CRYOMODULE DESIGN

The minimum superfluid helium layer covering the cavity wall should not be thinner than 5 mm. The volume of helium in the helium tank should be rationally minimized, if possible below 30 litre of helium per cavity (60 litre in total including liquid helium in the phase separator collector).

The combined cavity with helium tank assembly is to be designed to withstand pressure increase of ΔP of 2.6 bar without plastic deformation at ambient temperature. Safety devices should protect the cavity and the cryostat from such pressure rise situations. Design pressure for the

cryostat assembly should be based on installed safety devices according to their design rules; a cryostat equipped with a safety valve set at 1.8 bar and a rupture disc set at 2.2 bar). Both safety devices will be installed in the way to avoid potential projection of helium towards the passages or transport areas. Deflector installation is to be analyzed, but preliminary positions for the rupture disc and safety valve have been proposed on transfer line between the service module and cryostat – on the service module side.

7.2 CRYOGENIC INSTRUMENTATION

The cryostat should be equipped with following instrumentation:
1. Helium level measurement – each helium tank should be equipped with a level gauge, allowing for helium level measurement from the bottom through the phase separator (each gauge should allow for helium level regulation in the phase separator collector).
2. Pressure measurement on the saturated helium bath is to be provided (PT x 1),
3. Temperature measurement on each cavity helium tank is to be provided, installed on the bottom of each helium tank (suggested: CERNOX type transducer, TT x 2),
4. Electrical heaters of 50 W are to be installed on each helium tank (EH x 2)
5. Temperature measurement on 80 K line is to be provided (can be outside the cryostat, TT x 2 on inlet and outlet lines)

All sub atmospheric instrumentation/safety devices with ambient air interface will have to be equipped with appropriated helium guard.

7.3 HEAT LOAD BUDGET

The cavities are housed in individual titanium helium tanks connected by a 100 mm diameter two-phase He pipe placed above the cavities along with a 20 mm diameter cool down bypass lines placed below the tanks. The two phase pipe ensures that the liquid is fed to the cavities by gravity, and is also used as a pumping line for gaseous helium. A saturated helium bath maintains the cavities operating temperature at 2 K. Liquid helium is supplied to the two-phase pipe through 10 mm supply line. It is proposed to fill from one single point at extremity opposite to the pumping outlet of the two-phase pipe, and control He level about half of the two-phase pipe diameter.

The bottom bypass of 20 mm diameter will be used during cool down for parallel helium distribution to two helium tanks allowing for progressive cavities cool down from the bottom to the top. This bypass will have also the function to equilibrate the quantity of helium between two tanks in cases when two-phase pipe will be out of this function (transients – e.g. filling, special tests). The static plus dynamic heat loads are expected to be approximately 30 W to the 2 K bath for a two-cavity module. Table 12 shows the estimated contributions to the heat load to the cryogenic circuits at 2 K and 80 K for the two cryomodule. The cryogenic limits in the LHC are not precisely known at this time. However, the 15 W per cavity heat load at 2 K is small compared to the LHC heat load capacity; the total heat load of the LHC crab cavity systems is estimated at 0.5 kW at 2 K.

In the SPS the existing TCF20 refrigerator, running currently for COLDEX in SPS-LSS4, has too small capacity to compensate for the heat load of crab cavity SPS test. Due to the change of the location in the SPS to LSS6 a new strategy is put in place to install an adapted cold box at SPS surface or cavern near the BA6 region. The capacity of the new cold box will be specified to cover crab cavity static and dynamic heat losses including a contingency factor of 2.5 (at

least 70 W at 2 K). With this approach all operations at 4.5 K such as cool down and filling should be performed reliably. The first limitation from the new system is expected to be on low pressure helium pumping for normal operation at 3.5 g/s (~70 W at 2 K).

Table 12: Heat loads for a two-cavity cryomodule.

	DQW		RFD	
Static at >>	2K	80K	2K	80K
Radiation	1	35	1	35
CWT	0.2	2	0.2	2
Supports	0.6	5	0.8	5
Power Coupler	4	100	4	100
Instrumentation	1	0	1	0
HOM/Pickup	1.5	10	1	10
Tuner	0.3	10	0.3	10
Total static	8.6	162	8.3	162
Dynamic				
Cavity	6	0	6	0
FPC	5.6	10	8	20
HOM/Pickup	11.4	120	7.6	80
Beam	0.5	0	0.5	0
Total Dynamic	23.5	130	22.1	100
TOTAL	32.1	292	30.4	262

7.4   THERMAL LOSSES THROUGH THE THERMAL SCREEN

The thermal screen adopts MLI (Multi-Layer Insulation) in order to minimize the radiative heat exchange between the cold mass and the surroundings at 300 K. In the SPS, it is thermalized at 80 K with liquid Nitrogen for the SPS tests only. With this configuration, the heat exchange is lower than 1 W, as shown in Table 13.

For hosting the instrumentation necessary for the alignment measurements, holes will be machined in the thermal screen: this increases the heat losses to the cold mass, because of the high equivalent emissivity of the hole surface. To estimate this additional radiation loss, FEA have been performed for different holes configurations, as resumed in table Y.

COMPACT CAVITY CRYOMODULE

Table 13: Heat extra load due to alignment

Number and diameter of holes in the thermal screen	Additional heat losses to the cold mass
4x ⌀60mm + 16x ⌀30mm	1.9 W
4x ⌀60mm	1.1 W
4x ⌀50 mm + 16x ⌀26 mm	1.38 W
4x ⌀60 mm + 16x ⌀30 mm (and 50 mm-long tube around larger holes)	1.45 W

8   MAGNETIC & THERMAL SHIELDING

Degradation of the surface resistance of the superconductor (and hence the cavity Q) can occur due to trapped DC magnetic flux, and this can arise from stray fields in the vicinity of the cavity or from sources such as the earth's magnetic field. For any such external magnetic field, the contribution to the cavity surface resistance (assuming a RRR > 250), is estimated to be

$$\frac{R_{mag}}{\text{n}\Omega} = 3 \frac{\langle H_{ext}\rangle}{\mu\text{T}} \sqrt{\frac{f}{\text{GHz}}},$$

Assuming a geometric factor of approximately 100, R_{mag} has to be below 1-2 nΩ to maintain the total surface resistance to below 10 nΩ. To achieve this, magnetic shielding in the cryostat should reduce the external magnetic field on the outer surface of the cavity to below 1 µT field to achieve the desired quality factor of $Q = 1 \cdot 10^{10}$. For reference, in Central Europe the Earth's magnetic field has size of about 48 µT, with a horizontal component of 20 µT and a vertical component of 44 µT.

The crab cavity magnetic shielding consists of a 'warm' outer shield and two 'cold' inner shields. This double layer solution, comprising a 3 mm µ-metal (warm) and 1 mm nickel-iron alloy (cold), was determined to be the optimal solution for achieving the required specification with sufficient safety margin. Both inner and outer shields feature several penetrations, for cavity ports, supports, and interfaces, which affect the shields performance. Care is then taken to minimise the size and number of penetrations. Additionally, branch cover tubes have been utilized, where feasible, to attenuate the field leak through holes.

A magnetic survey in the SPS area concluded that an external field of no more than 200 μT is to be expected during operation [27]

8.1   WARM MAGNETIC SHIELDING

The external warm magnetic shield is made of 3 mm thick µ-metal and is directly attached to the vacuum vessel. Figure 32 shows analysis performed in OPERA of the magnetic field amplitude inside a 2-cavity CM for an applied external shield of 200 μT in the longitudinal direction (parallel to the beam axis).
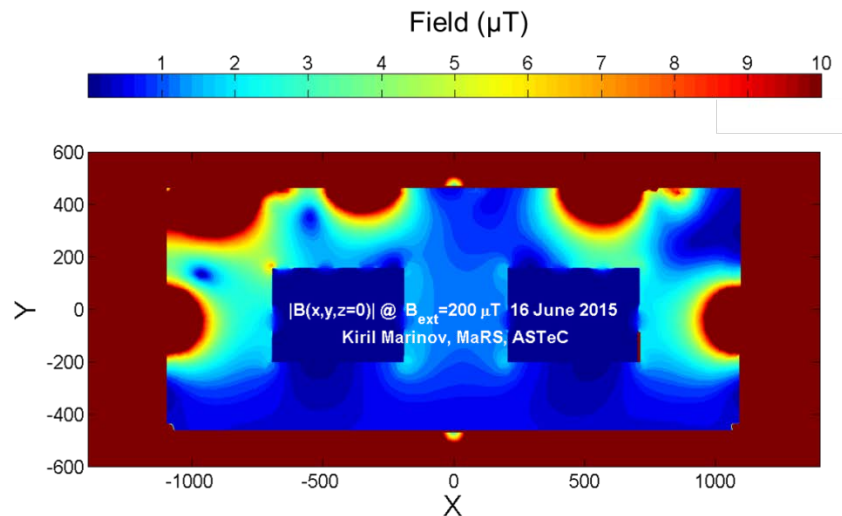
Figure 32: Magnetic field amplitude inside the 2-cavity CM with the 2nd internal cold magnetic shield, scale 0 to 10 µT (top). An external field of 200 µT in the direction parallel to X (longitudinal) is used.

8.2   COLD MAGNETIC SHIELD

Due to the large apertures in the shielding for couplers and beam pipes this layer on its own is not sufficient to shield completely the Earth's magnetic field to the required level and with sufficient safety margin. Therefore, a second shield is foreseen close to the cavity. Assuming the worst-case field orientation – parallel to the cryomodule longitudinal axis – the analysis shows that the use of the proposed two-layer shielding solution to achieve magnetic fields well below 1 µT is feasible, as shown in Figure 32, [28].

In order to reduce the size of the holes in the internal shield the cold magnetic shield is integrated inside the helium vessel as presented in Figure 33. The internal shield is a 1 mm thick Cryoperm or Aperam Cryophy.

8.3   ASSEMBLY PROCEDURE AND MECHANICAL STRENGTH

Since the shield is located inside and supported from thick walled helium vessel, the assembly procedure for both shield and tank requires careful consideration and planning. Figure 33 shows some of the assembly stages for the cold DQW shield within the helium vessel. Firstly, the split bottom panels are assembled around the cavity before both are mounted to the helium vessel base plate. Thereafter, the remaining shield panels can be assembled around the cavity along with the connecting strips and branch tube covers. Once the shield assembly is complete, the front, rear and top vessel plates can be assembled so that the remaining shield supports can be connected. Finally, the side plates can be fastened and the vessel is made leak tight with thin walled strips being welded over the bolt connection slots [29].
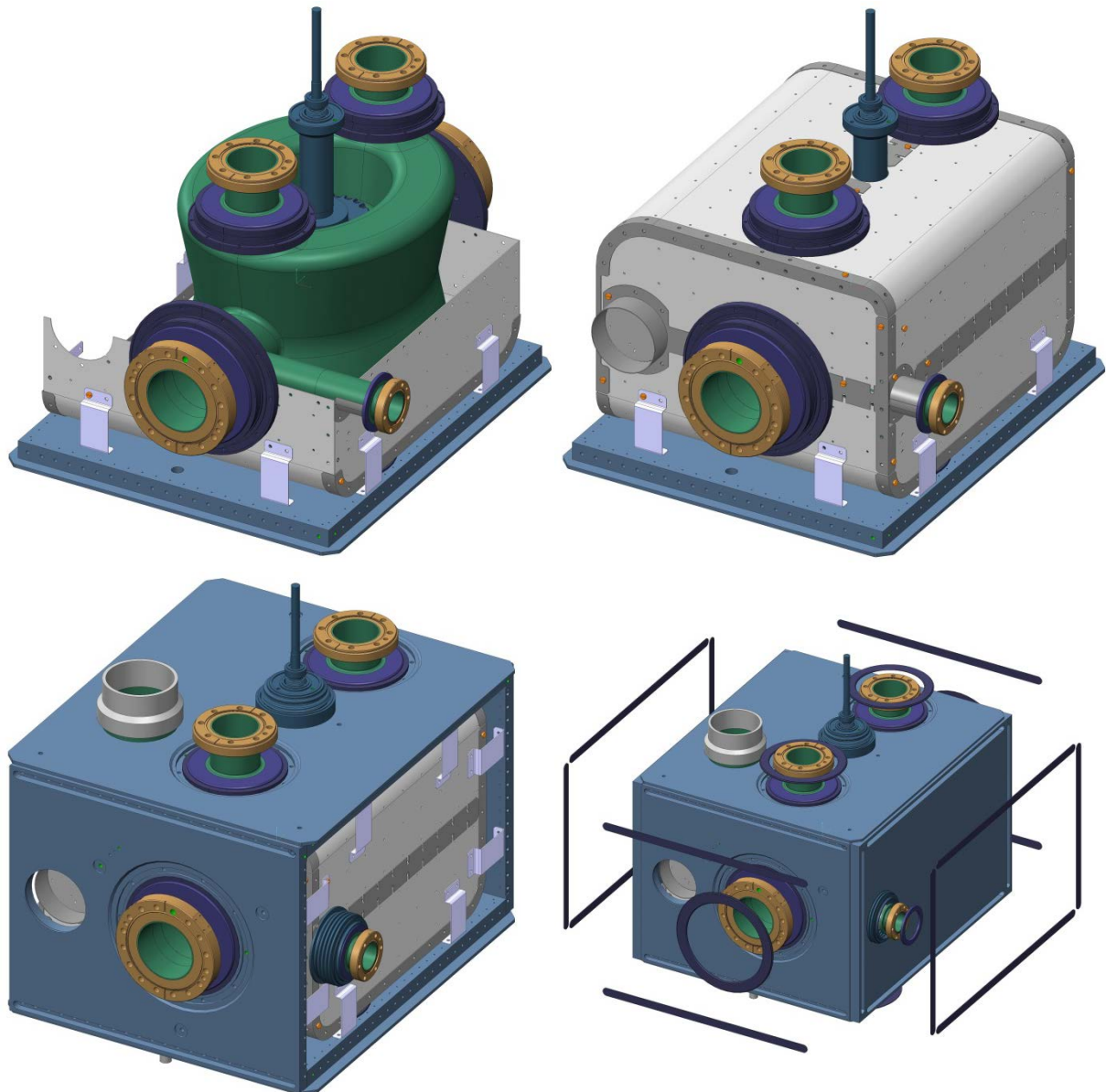
Figure 33: Some stages during the assembly of cold magnetic shield inside the helium vessel

Magnetization of materials for both cold and warm shield is adversely affected by stresses. Hence, degradation of the magnetic properties during assembly and handling should be carefully studied and monitored. Effects of weight and thermal stresses are also modelled in ANSYS, Figure 34, [30].

The simulations indicate that while the maximum stress is 373 MPa in the Ti supports, the stress on the shield is minimised and well below the shield elastic limit (~150MPa). The supports are designed to give sufficient flexibility in order to eliminate any thermal stresses on the shield. Even elastic stresses, may reduce permeability which, at worst, is comparable to a penetration of equivalent size. As such it is important that the difference in thermal contraction between the helium vessel and shield is carried by the titanium mounts which increases in strength at cryogenic temperatures. The maximum stress in the mounts is purely localised at the fastener

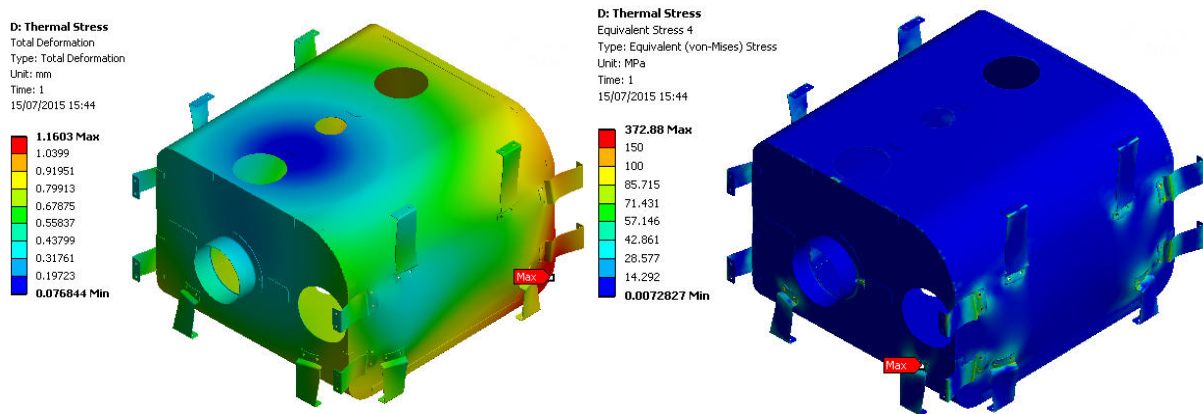connection and is likely to be lower since the model is somewhat over constrained for conservative results.

Figure 34: Thermal contraction and stress of DQW magnetic shield from room temperature to 2K

8.4 THERMAL SHIELDING

The thermal shield is made of rolled aluminium sheets. The shield is suspended from the vacuum vessel via flexible guides made from titanium alloy that also copes, through angular movements, with its thermal contractions. The absence of mechanical contact between the shield and the string of cavities eliminates the risk of interference with the alignment of the cavities induced by differential contractions and cooling transients. The cryomodule contains a single thermal shield, actively cooled in the LHC between 50 and 80 K by a cryogenic cooling line containing pressurized helium gas. For the SPS tests, similar solution using pressurized He will be applied and will replace initially foreseen N_2 circuit. A 30-layer prefabricated Multi-Layer Insulation (MLI) blanket protects the thermal shield whereas a 10-layer blanket is mounted around each helium vessel.

9 CRYOMODULE AND VACUUM VESSEL

The sum of all the systems to be installed in SPS and later in LHC is called cryomodule. The most external layer of the cryomodule is the vacuum vessel that provides a safe space to the hardware inside and contains vacuum in order to isolate the He tank thermally.

Major constraints in the design of this vessel are the integration steps, i.e. the shape and the openings must allow the assembly and positioning of all the system in their right location. On top of that, the dimensions of the tank depend on the maximum dimensions of the envelope, including the systems outside the vacuum vessel, Figure 35:

- 2900 mm longitudinally for the RFD, 2750 mm for the DQW
- 1050 mm laterally (and proper position with respect to the beam for both axis)
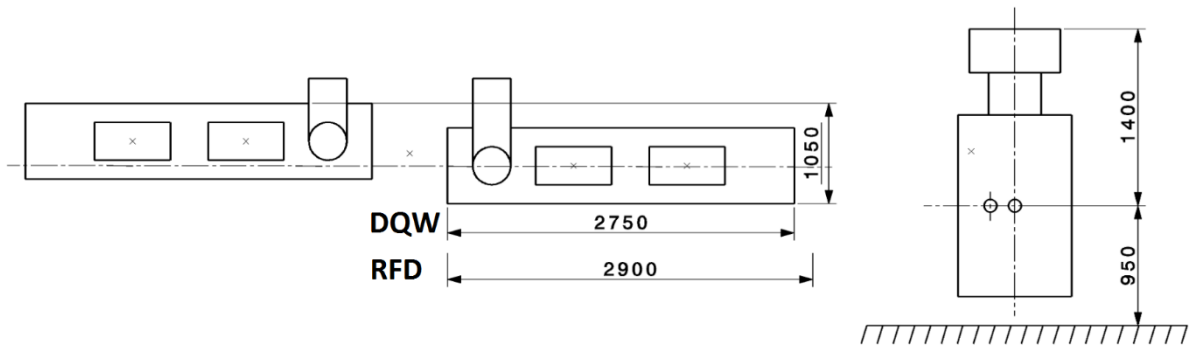- 2350 mm height (1400 mm above the beams, 950 mm below)

Figure 35: Maximum envelope for the two-cavity cryomodules.

The detailed design also depends on the deformation induced by the difference of pressure between the outside (atmosphere) and the inside (vacuum) that should not induce any excessive deformation or instability, especially at the interface with the dressed cavity through the support and alignment system or the beam axis.
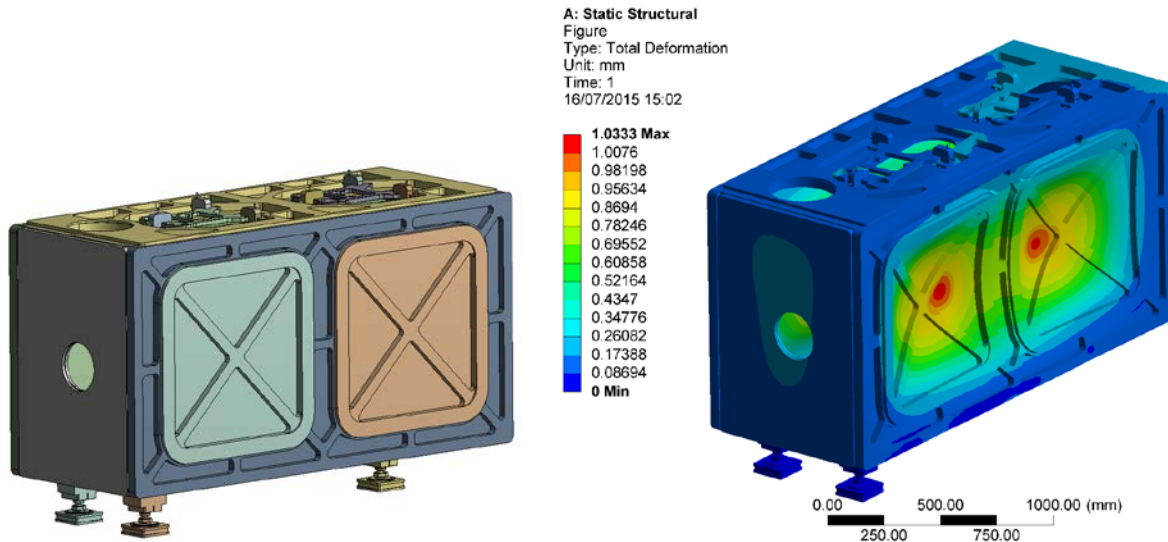

Figure 36: Preliminary design of the vacuum vessel (left), deformation of the vessel when loaded with internal vacuum and weight of the dressed cavity (right)

The use of ribs is foreseen in order to keep the deformation under control without incurring in problems due to an excessive mass. The exact shape and configuration of these ribs is under definition. Preliminary calculations, however, show that the deformation at the interface with the cavity support is about 100 µm, Figure 36. The thickness of the plates (in stainless steel) is 15 mm outside the ribs and 50 mm at the ribs.

10   RF POWERING & CONTROL ARCHITECTURE

The overall architecture and approximate volume of the RF infrastructure is schematically shown in Figure 38. Near Point 1 and 5, the existing caverns closest to the cavity (RR caverns) are approximately 80 m away while requiring large space in the tunnel to pass the RF transmission lines along this distance. Radiation concerns rule out the installation of highly sensitive RF electronics in those caverns.
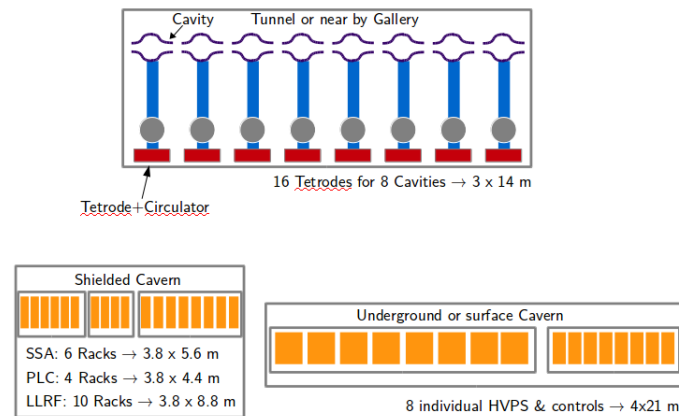
Figure 37: Schematic of the RF system layout in (a) the LHC tunnel; (b) the electronics racks in a shielded cavern close to the cavities; (c) the surface building. Note that these are only estimated values of space requirements.

Therefore, two remaining options are under study:

<u>RF gallery near crab cavities</u>: The longitudinal range would be approximately at 155 m from IP1 and IP5 on either side in a gallery parallel to the LHC tunnel. Access to the gallery is required with RF ON and field in the cavity but without circulating beam. This is assumed as the present baseline under the double decker layout with a parallel gallery just above the LHC tunnels is used to place the RF services (see Figure 38).

<u>Surface Option</u>: This option is similar to that of the near RF gallery but all RF services located on the surface which is approximately 100m vertically up from the LHC tunnel. The longitudinal range is similar as above, preferably above the crab cavity locations on the surface on either side of IP1 and IP5. To minimize the high power RF transmission line dimensions, the circulator and load is assumed to be in an extended tunnel alcove close to the cavity.

An independent powering system using LEP-type 400 MHz tetrodes (or an equivalent IOT) of (40…80) kW is assumed. Recent advances in solid state technology could eventually lead to power sources in the required power range and may provide a cheaper and more robust platform. The tetrodes provide adequate power overhead in a compact footprint. This scheme also would allow for a fast and independent control of the cavity set point voltage and phase to ensure accurate control of the closed orbit and the crossing angle in the multi-cavity scheme. Most importantly, the fast control of the cavity fields will minimize the risk to the LHC during an abrupt failure of one of the cavities to ensure machine protection before the beams can be safely extracted. For such a fast and active feedback, a short overall loop delay between the RF system and the cavity is required [12].

To provide a strong feedback, the low level RF system requires the total loop delay to be approximately $1-2$ μs. This includes the group delay of the driver, amplifier, circulator and cable delays. Therefore, a distance less than 100 m is desired for the separation between the amplifier, electronics and the cavity in the tunnel. Such a short delay is already in place for the ACS main RF system in Point 4 (650 ns loop delay) with a service gallery running parallel to the tunnel.

The controls and driver electronics are required to be located in a radiation minimized zone. Assuming two tetrode amplifiers per cavity to provide the 80 kW and electronic racks required for drivers, PLC, LLRF and fast interlocks for 8 cavities per IP side, an area of approximately 100 m² is needed near the cavities. The high-voltage power supplies and the power controls would need an additional 85 m² which will nominally be placed on the surface. If all high and

low power RF and controls are placed on the surface, an equivalent of 185 m² will be required there. The proximity of the circulator and RF loads to the cavity will allow for smaller RF transmission lines from the surface to the tunnel.
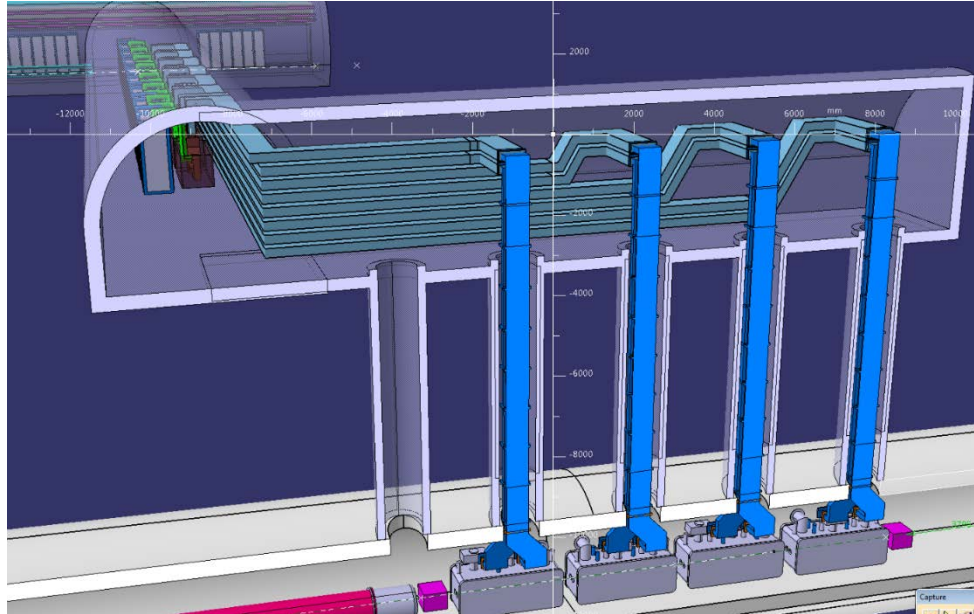

Figure 39: Preliminary sketch of a high-power RF, controls and LLRF layout in a surface building, distributed over two levels. Lower level containing pumps and general services, upper level containing RF amplifiers and equipment racks (courtesy C. Magnier, P. Fessia).

A total height of approx. 6 m is estimated for the high power RF, controls and services, distributed over two levels. This allows a minimum space of 3 m for the equipment racks, amplifiers etc. while leaving 3 m height directly underneath cooling pumps, cabling and services, see Figure 39. Alternatively, additional volume adjacent to the building to accommodate the pumps, ventilation and other required units for high power amplifiers can be envisioned to limit the height. All "surface" building could actually be underground and would not occupy any surface area. The required electrical interfaces are specified in Ref. [36]. A study is ongoing to determine the feasibility of the civil engineering with minimal perturbation to the LHC running [37].

10.1 LLRF ARCHITECTURE AND OPERATIONAL SCENARIOS

The RF control system, also commonly referred as the low level RF system (LLRF) includes several functionalities. First, a tuning control is required to keep the cavity resonant frequency on-tune with the beam during the crabbing operation. If required, the LLRF also has to ensure that the cavity is safely parked at an optimal detuned position during filling, ramping and collisions without crabbing. This system also synchronizes the phase of the RF kicks with the exact passage of the bunches for both beams. The LLRF includes a regulation loop around the amplifier (to reduce the RF amplitude noise and phase noise in a band extending to few tens of kHz), plus an RF feedback to control the cavity field precisely. The feedback loop consists of both a local loop around the cavity-amplifier and a global loop regulating the vector sum of voltages on the two sides of the interaction regions. The global loop will reduce beam perturbation following a single cavity trip, by quickly reducing the field in the companion cavities to track the uncontrolled voltage in the faulty cavity. The beam dump system has a 3-turns (270 μs) response delay.

For each ring, the eight accelerating cavities (ACS system) are driven from a single reference generated in a surface building above IP4. These two signals must be sent over phase-compensated links to IP1 (ATLAS) and IP5 (CMS). The eight crab cavities of a given ring at each IP are coupled with an 8-IN, 8-OUT multi-cavity feedback (MFB). Figure 40 shows the proposed architecture.
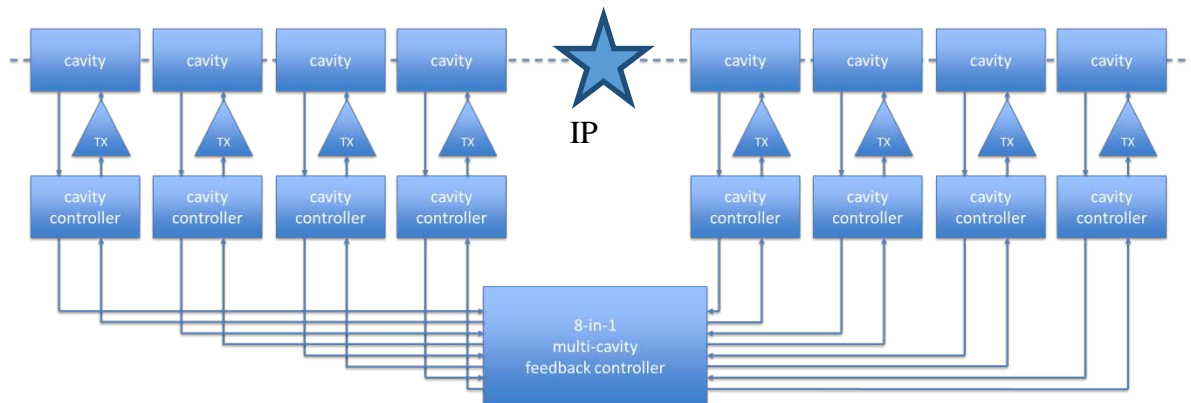

Figure 40: Proposed LLRF architecture for one ring at one IP.

Per ring and IP, a central controller receives measurements from all relevant cavities and makes corrections to the drive of all individual TX. If the field starts changing in a cavity, the MFB will adjust the field in the other cavities on both sides of the IP, such that the orbit distortions remain local. As described in 2.6, on flattop, counter-phasing is nulled while keeping the voltage set point small. The RF feedback keeps the cavity impedance small (beam stability) and compensates for the beam loading as the cavity moves to resonance. The voltage set points are ramped to synchronously change the voltage in all crab cavities as desired. Any levelling scheme is possible. With a circulator between amplifier and cavity, the TX response is not affected by the cavity tune.

At present the spacing between LHC bunches within a batch is strictly constant along the ring. A large amount of RF power is used in the ACS system to fully compensate the transient beam loading caused by the 3 µs long abort gap and the smaller gaps required for the injection kicker ("half detuning"). This scheme cannot be extended into the HL-LHC era as it would require excessive RF power. The power required is minimized by optimally detuning the cavity ("full detuning") and adapting the cavity set-point phases bunch by bunch. It results in bunch arrival time modulation of up to ± 42 ps [38]. This may be acceptable given the 1 ns bunch length. There is no effect on the luminosity as the modulation is identical in both beams, only vertex position is modulated around the nominal vertex by a maximum of 1 µm over 1-turn. The bunch to bunch variation within a batch is at least an order of magnitude smaller. If not, the LLRF must synchronize the bunch-by-bunch crabbing field with the actual phase modulation.

10.2 CAVITY FAILURE SCENARIOS

Crab cavity failures can lead to a fast voltage and/or phase change with a fast time constant. This can lead to large, global head-tail oscillations or coherent betatron oscillations with a change in transverse beam trajectories of $1.7\,\sigma$ for a single cavity failure; the effect is cumulative with the number of failing cavities. These failures can be broadly classified into two categories: i) fast failures, single or few turns (for example a sudden cavity quench or

breakdown); ii) slow failures, several tens of turns or greater (caused by vacuum degradation, voltage and phase drifts or similar). The slow failures can be "easily" dealt by suitable beam interlock system, so in the following we discuss the fast failures.

Due to the relatively high quality factor in the superconducting cavity, the stored energy inside the cavity can typically only be extracted with a time constant determined by Q_L, which results from the strong coupling to the cavity via the power coupler. The stored energy will decay with a time constant $\tau = 2Q_L/\omega_0$. For a $Q_L = 5 \cdot 10^5$, the time constant is approximately 400 µs. The three turn delay time (267 µs) for a beam dump trigger is an important consideration during a RF source failure, where the cavity stored energy decays to roughly half its value before the beam can be safely aborted. In the case of a quench, the time constant of field decay may be dominated by the quench dynamics rather than Q_L. The situation is similar due to strong and sudden electron loading due to multipacting or other phenomena.

The cavity quench mechanism described above and measurements from KEKB crab cavities [39] indicate that a quench typically is a slow thermal process (typically of the order of several milliseconds). Once the temperature on a sufficiently large area exceeds the critical temperature of Niobium, the quench can propagate very fast to completely quench or cause RF breakdown. However, any change in cavity quality factor already well before reaching a critical temperature limit could be easily detected from the requested forward power (fast) or changes in the cavity temperature bath (slow). An interlock on the forward power, except due to operationally induced orbit excursion, can cut the RF to slow down or stop the quench propagation. A beam abort if required can be triggered simultaneously (a few µs) for machine protection. Therefore, a thermal quench is not considered detrimental within the machine protection reaction time.

10.3 FAILURE SCENARIOS MITIGATION

The choice of low operation temperature (2 K) and moderate surface field levels allows operation with ample margin from quench temperature and field limits. The significantly better thermal conductivity of superfluid Helium should also improve the thermal performance and stability of the cavity. Additional measures in the cryomodule design are being considered to dimension the Helium enclosures with sufficient margin for heat flux. The cavity thermal and RF stability will be thoroughly tested in the SM18 test facility and during the SPS beam tests.

To minimize the perturbation on the beam during a cavity failure, the MFB will adjust the field in the other cavities on both sides of the IP, such that the orbit distortion remains local. Figure 41 shows the cavity control of two cavities across the IP with one cavity failure and the RF controller to adjust the second cavity to follow. The rapid change in field will also result in a detuning of the cavity, however, the mechanical tuning system is -unable to adjust the tune within 400 µs. Since a rapid breakdown of a failed cavity may become unpredictable, it is probably safest to ramp down the cavities synchronously. However, small and slow changes in one of the cavities can be adjusted without aborting the beam.
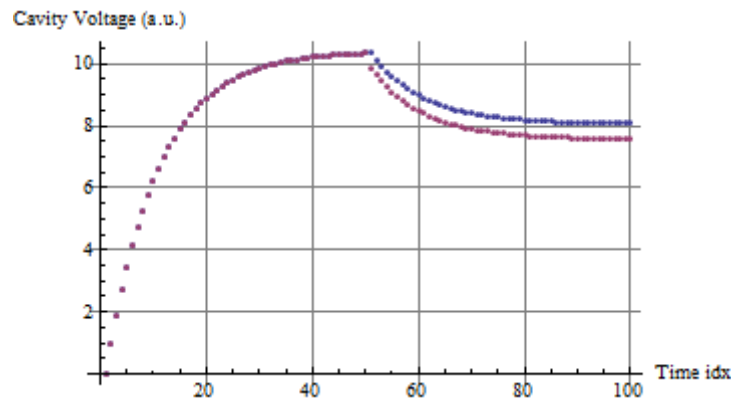
Figure 41: Voltage response with strongly coupled cavities across the IP as a function of time [µs]. At 50 µs, one cavity trips (red trace) and the other one is forced by the RF controller to follow (blue trace).

The cavities can be equipped with fast tuning system such as a piezo mechanism. If the speed of such tuning devices is sufficient, it could compensate for Lorentz force detuning during transients and thus keeping the tune within the bandwidth of the feedback system.

An additional mitigation to avoid large beam losses (and hence deposited energy) in case of single or multiple cavity failure is a robust measurement and interlocking of the halo population and eventual head-tail oscillations. This could be achieved with new equipment such as a hollow electron lens for cleaning of the bunch halo and interlocking with improved diagnostics like fast head-tail monitors and/or fast beam loss monitors (diamond, e.g.).

11 FUTURE PLANS

An essential milestone for a crab cavity is the test in the SPS, planned to demonstrate reliable operation, machine protection, cavity transparency and to understand the long term effects on hadron beams. All RF manipulations and cavity-beam interactions will be first validated and commissioned in the SPS with a prototype two cavity crab cavities system. The prototype cryomodules, RF services and infrastructure are in advanced stage with an installation in the SPS foreseen for the winter shutdown of 2017-18.

Immediately after the validation of the SPS cryomodule, a LHC pre-series (aka production prototype) cryomodule for the two types will commence the design and fabrication phase to address the specific LHC interfaces. Only a minimum number of changes to accommodate integration aspects in the LHC and the cryomodule design is expected to largely remain the same as SPS. Upon RF validation of the LHC pre-series, the construction of the 16 modules (2-cavities each) will commence. The cryomodules are expected to be sequentially completed with comprehensive tests on the surface prior to their installation in the LHC tunnel in LS3.

COMPACT CAVITY CRYOMODULE

Doc. Identifier:
HILUMILHC-Del-D4-4-v2.0

Date: 06/11/2015

12 ACKNOWLEDGEMENT

13 REFERENCES

[1]   A. Piwinski, Nucl. Instr. and Meth. 81, 199 (1970).

[2]   R. Palmer, Energy scaling, crab crossing and the pair problem SLAC-PUB-4707, 1988.

[3]   K. Oide, K. Yokoya, The crab crossing scheme for storage-ring colliders, SLAC-PUB-4832.

[4]   Y. Funakoshi, Operational Experience with Crab Cavities at KEKB, http://arxiv.org/pdf/1410.4036

[5]   S. Fartoukh, Pile up management at the High Luminosity LHC and introduction to the crab kissing concept, CERN-ACC-2014-0076 (2014).

[6]   G. Arduini et al., Summary of the LHC-CC11 Crab Cavity Workshop, CERN-ATS-2012-055, 2011.

[**7**]   S. De Silva et al., in the proceedings of IPAC13, Shanghai, 2013.

[8]   B. Hall et al., in the proceedings of IPAC12, New Orleans, 2012; G. Burt et al., in the proceedings of IPAC13, Shanghai, 2013.

[9]   R. Calaga et al., in the proceedings of IPAC13, Shanghai, 2013; Q. Wu et al., in the proceedings of IPAC13, Shanghai, 2013.

[10]   A. Yamamoto et al., Crab cavity system external review report, CERN-ACC-2014-0093, 2014.

[11]   R. Calaga, A. Ratti, Presented at the 4th HiLumi Meeting, KEK, 2014.

[12]   P. Baudrenghien, presented at the 2nd HiLumi Meeting, Frascati, 2012.

[13]   P. Baudrenghien et al., Functional specification of the LHC prototype crab cavity system, CERN-ACC-Note-2013-003, 2013.

[14]   R. Calaga, B. Salvant, Comments on crab cavity HOM power, CERN-ACC-NOTE-0024.

[15]   N. Biancacci et al., HL-LHC impedance and stability studies, presented at the 4th HiLumi workshop, KEK, 2014.

[16]   VDI 2230 Part 2 – Systematic calculation of highly stressed bolted joints / Multi bolted joints, published by Beuth in 20014-12

[17]   VDI 2230 Part 1 – Systematic calculation of highly stressed bolted joints / Joints with one cylindrical bolt, published by Beuth in 20014-12

[18]   EN 13445-3:2002, Unfired pressure vessels - Part 3: Design

[19]   Website: http://www.mitcalc.com/doc/welding/help/en/welding.htm (Access: 30.06.2015).

[20]   F. Cerutti, L.S. Esposito: Energy deposition for HL-LHC v1.1: TAN/D2/Q4 (http://indico.cern.ch/event/326148/session/17/contribution/43/attachments/633143/871389/2014-11-20_TCLX4.v2.key.pdf), p. 34,35

[21]   http://www.npl.co.uk/science-technology/dimensional/frequency-scanning-interferometry-research

[22]   BCAM "Brandeis CCD Angle Monitor", http://alignment.hep.brandeis.edu

[23]   P. A. Coe, A. Mitra, S. M. Gibson, D. F. Howell and R. B. Nickerson, "Frequency Scanning Interferometry- A versatile, high precision, multiple distance measurement technique", proceedings of the 7th International Workshop on Accelerator Alignment, 2002

[24]   http://www.etalon-ag.com/produkte/absolute-multiline-technologie/

[25]   J.-C. Gayde; Y. Kadi; G. Kautzmann; Y. Leclercq; S. Waniorek; L. Williams, HIE ISOLDE alignment and monitoring system. Technical Design and Project Status, International Workshop for Accelerators Alignment, IWAA 2012

[26]   S. Waniorek, "A Software Solution for the Alignment of the HIE-ISOLDE Accelerator at CERN", Master Thesis HS Karlsruhe, CERN (2012)

[27]   J. Bauche, A. Macpherson, Estimate of Ambient Magnetic Field in the SPS Crab Cavity Location, CERN, 2014

[28]   K. Marinov, Assessment of the magnetic shielding requirements for Hi Lumi Crab Cavities, Hi-Lumi progress review meeting, STFC Daresbury, August 2014

[29]   R. Leuxe, LHC Crab Cavity Helium Tanks Mounting Sequence, Helium Vessel Design Review, CERN, 5 May 2015

[30]   N. Templeton, Cryogenic Magnetic Shields, Helium Vessel Design Review, CERN, 5 May 2015

[31]   R. Calaga, B. Salvant, Comments on crab cavity HOM power, (unpublished).

[32]   M. Navarro-Tapia, R. Calaga, A. Grudiev, RF mulipoles from crab cavities, IPAC13, Shanghai, 2013.

[33]   K. Brodrinski, S. Claudet, Private communication.

[34]   S. Pattalwar et al., Key Design features of the Crab-Cavity cryomodule for HI-LUMI LHC, in the proceedings of IPAC14, Dresden, 2014.

[35]   T. Jones et al., Crab cavity manufacturing readiness meeting, CERN, 2014.

[36]   L. Arnaudon et al., Conceptual specification of the crab cavity RF system, EDMS 1363181.

[37]   P. Fessia et al., Private communication.

[38]   R. Calaga, Chamonix 2014, in the proceedings of Chamonix 2014 (to be published).

[39]   K. Nakanishi et al., in the proceedings of IPAC10, Kyoto, 2010.

[40]   R. Calaga et al., Conceptual specification of the LHC RF harmonic system, EDMS 1363179.

[41]   E. Montesinos, Private communication.

[42]   E. Shaposhnikova, presented 4th HiLumi Meeting, KEK, 2014.

[43]   O. Bruning et al. (ed.), LHC Design Report, CERN-2004-003, CERN, Geneva (2004), p. 140-142.

[44]   W. Hofle , D. Valuch, Transverse Feedback: high intensity operation, AGC, IGC, lessons for 2012, LHC Beam Operation Workshop, Evian, December 2011, CERN-ATS-2012-083, CERN, Geneva (2012), p. 97-100.

[45]   W. Hofle, Transverse Feedback Systems in LHC and its Injectors: Projected Performance and Upgrade Paths, 3rd CARE-HHH-APD Workshop, LHC-Lumi-06, Valencia, 16-20 October 2006, CERN-2007-002, CERN Geneva (2007), p. 177-179.

[46]   CERN CDD Drawing LHCLJ4GA0007 AH, March 2007

[47]   W. Hofle, G. Kotzian, T. Levens, D. Valuch, Transverse Feedback, 5th Evian Workshop, 2-4 June 2014, CERN Geneva (2014).

[48]   R. J. Steinhagen, M. J. Boland, T. G. Lucas, A Multiband-Instability-Monitor for High-Frequency Intra-Bunch Beam Diagnostics, Proc. IBIC 2013, Oxford UK (2013), 327-330.

[49]   W. Hofle, F. Dubouchet, G. Kotzian, D. Valuch, Performance of the LHC Transverse Damper with Bunch Trains, Proc. IPAC 2013, Shanghai (2013), p. 3022-3024.

[50]   J. R. Thompson et al., Initial Simulation of Damping System for Electron Cloud Driven Instabilities in the CERN SPS, Proc. PAC 2009, Vancouver (2009), p. 4713-4715.

[51]   J.D. Fox et al., First Results and Analysis of the Performance of a 4 GS/s Intra-Bunch Vertical Feedback System at the SPS, Proc. IPAC 2013, Shanghai (2013), p. 3070-3072.

[52]   J. M. Cesaratto et al., SPS Wideband Transverse Feedback Kicker: Design Report, SLAC-R-1037, SLAC (2013); M. Cesaratto et al.*,* A Wideband Slotted Kicker Design for the SPS Transverse Intra-Bunch Feedback, Proc. IPAC 2013, Shanghai (2013), p. 3073-3075.

14   GLOSSARY

Acronym	Definition
ACF	Superconducting Crab Cavity
CM	Cryomodule
IP	Interaction Point
IR	Interaction Region
LEP	Large Electron-Positron Collider
LHC	Large Hadron Collider
RFD	RF Dipole Cavity
DQW	Double Quarter Wave cavity